CERN-ACC-NOTE-2019-0052

5 December 2019
guido.sterbini@cern.ch

MD2202: compensating long-range beam-beam effect in the LHC using DC wires

G. Sterbini, D. Amorim, G. Arduini, H. Bartosik, R. Bruce, X. Buffat, L. Carver, G. Cattenoz, E. Effinger, S. Fartoukh, M. Fitterer, N. Fuster-Martinez, M. Gasior, M. Gonzalez-Berges, A. Gorzawski, G.-H. Hemelsoet, M. Hostettler, G. Iadarola, R. Jones, D. Kaltchev, N. Karastathis, S. Kostoglou, I. Lamas-Garcia, T. Levens, A. Levichev, L. E. Medina-Medrano, D. Mirarchi, J. Olexa, P. S. Papadopoulou, Y. Papaphilippou, D. Pellegrini, M. Pojer, L. Ponce, A. Poyet, S. Redaelli, A. Rossi, B. M. Salvachua Ferrando, H. Schmickler, F. Schmidt, K. Skoufaris, M. Solfaroli Camillocci, R. Tomás-Garcia, G. Trad, A. Valishev, D. Valuch, C. Xu, C. Zamantzas, P. Zisopoulos.
CERN, CH-1211 Geneva, Switzerland

Keywords: LHC MD; beam-beam effect; long-range compensation; DC wire; MD2202.

Summary

This note summarizes the program of the LHC Machine Development to assess the potential and limits of the long-range beam-beam compensators held in 2017 (MD2202). Two compensator prototypes were installed in the machine during the EYETS16-17 and the first evidence of compensation were observed during the MD block 1 (FILLS 5898 and 5900, 9 h assigned on 1^{st} of July 2017). This study was also scheduled for the MD block 3 but could not be performed due to the machine unavailability (9 h assigned, 2 h available but unfortunately not exploitable for measurements). In MD block 4 an additional slot was scheduled (FILLS 6434 and 6435, 10 h on 29^{th} November 2017).

Contents

1 Introduction

One of the limits for the present LHC and HL-LHC performance is the electromagnetic interaction between the counter-rotating beams in the shared sections of the machines (beam-beam head-on, HO, and long-range, LR, interactions). Experimental studies on the effect of the BBLR were performed during several MDs in the past years [1, 2, 3, 4, 5] in conjunction with a regular follow-up and scrutiny of the BBLR impact on the operational machine performance [6, 7].

A solution to counter-react and alleviate the LR interactions was proposed in [8] and further developed in [9]. It consists in compensating the LR pattern (averaged along the beam filling scheme) by using DC wires.

In order to validate experimentally this approach and its approximations, two beam-beam compensation wires (BBCW) were installed in the LHC during the EYETS16/17 [10] in both sides of the IP5 for the Beam 2 (see Figure 1). There are in total four wires embedded in the TCL.4L5.B2 and TCTPH.4R5.B2 jaws (each of the two collimator jaws contains one wire, indicated as internal, "I", and external, "E", wire depending on whether the wire is between the two beam vacuum chambers or not). In the LHC layout sequence there are 8 markers for the 4 wires (two per wire indicating its downstream, D, and upstream, U, position). They are referred as

- BBCWE.4L5.U.B2, BBCWE.4L5.D.B2,
- BBCWI.4L5.U.B2, BBCWI.4L5.D.B2,
- BBCWE.4R5.U.B2, BBCWE.4R5.D.B2,
- BBCWI.4R5.D.B2, BBCWI.4R5.D.B2.

The BBCWI.4R5 and BBCWI.4L5 are connected respectively with the power converters (PCs)

- RPMC.UL557.RBBCW.R5B2,
- RPMC.USC55.RBBCW.L5B2.

These power converters are identical 4-quadrants converters rated for 40 V $\times$ 600 A. Due to the thermal constraints on the wire itself (ohmic losses) the maximum current in the wire has an operational limit at 350 A. A schematic of the installation is shown in Figure 1. During the 2017 MD only the internal wires were connected to the PC: only the internal wires can compensate all the RDTs (the wires are on the same side of the strong beam, B1). The compensation current has to flow opposite to the Beam 1 direction (compensation polarity). During the 2017 the power converters were configured only for positive current values since the wire hardware interlock could not handle negative current (this limit was removed during the YETS17-18).

The MD hardware and experimental program was discussed during two dedicated mini-workshop in 2015 [12] and 2017 [13].

We show in Figures 2 and 3 the main parameters of the wire geometry. It is important to note that the wire center is shifted by 3 mm with respect to the surface of the jaw. This

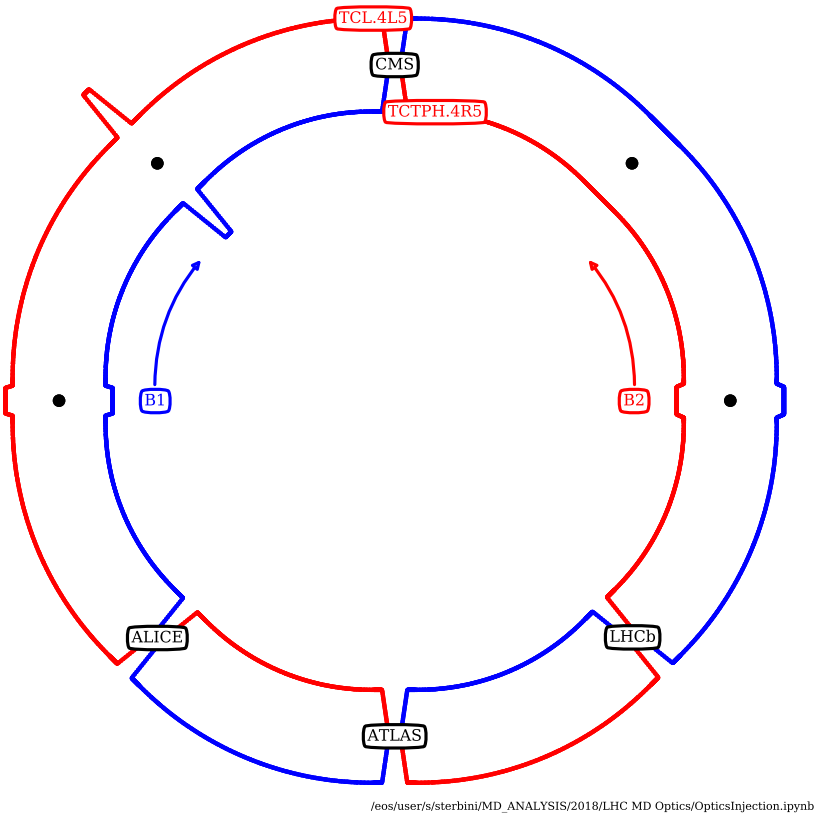

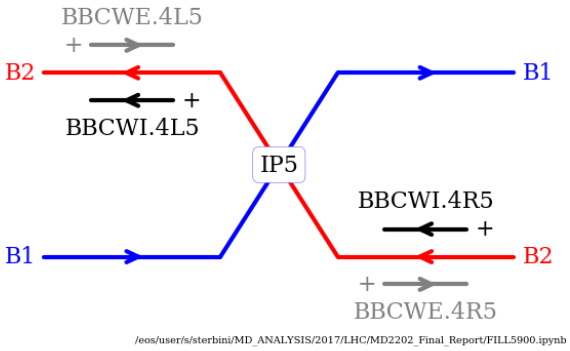

Figure 1: The wire installation in Interaction Region 5 (CMS).

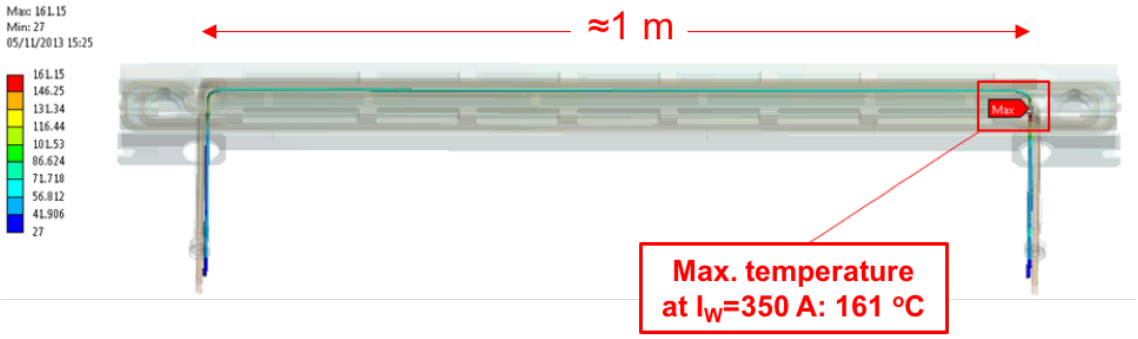

Figure 2: Top view of the wire in collimator prototype, courtesy of F. Carra [12].

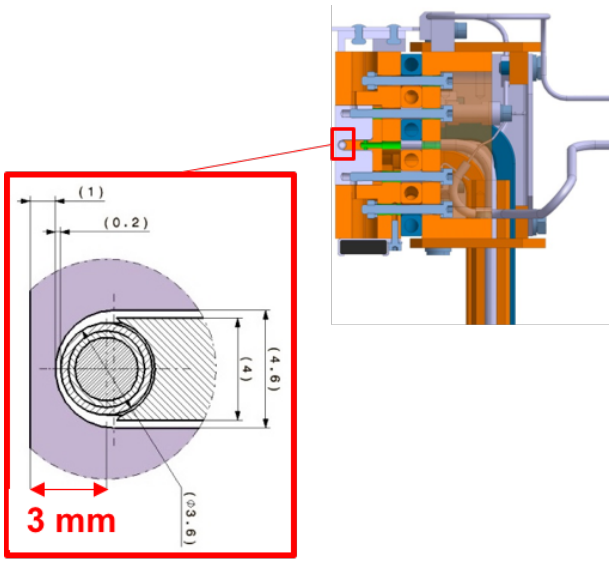

Figure 3: Top view of the wire in collimator prototype, courtesy of F. Carra [12]. It is important to note that the wire center is shifted by 3 mm with respect to the surface of the jaw.

implies that the minimum wire distance to the beam is the closest allowed setting of the jaw, therefore +3 mm.

The scripts used for data analysis of the MD are available on the public folder [14].

The results of this MDs were presented in several meetings and workshops [6, 15, 16].

1.1 Objective of the MD

As reported in details in [9], the LR interaction between the two beams can be approximated, assuming a weak-strong regime (Beam 1 in our case is the strong beam) and non-overlapping halos during the LR encounters, observing that the **electromagnetic** kick provided by Beam 1 on Beam 2 is equivalent to the kick given by a series of **magnetostatic** multipoles. Along the Interaction Region (IR), the interplay between the optics property of Beam 2 and the multipoles originated by Beam 1 gives rise to Resonant Driving Terms (RDT's) exciting Beam 2. One can dimension one DC wire to compensate part of these RDT's. Given the anti-symmetry of the IR optics, it is shown in [9] that with 2 wires positioned symmetrically with respect to the Interaction Point (IP, at $\pm s_W$) and at the same physical distance from the Beam 2 (d_W) and same wire current (I_W), one can correct 4 RDT's in the form (p1,q1)+(p2, q2) and, for symmetry, (q1,p1)+(q2, p2). In [9] one find the closed formulas to dimension d_W and I_W as function of p1,q1, p2 and q2 for a given LR encounter pattern (RDT's) assuming ideal phase advance between the LR and the wires. A posteriori, one can evaluate the effect of the non-ideal phase advance and eventually optimize d_W and I_W via numerical methods.

A very remarkable numerical evidence reported in [9] shows that, for a convenient choice of s_W, most of the RDT's are minimized. This observation opens the way towards a full compensation of the RDTs using 2 wires per IR as a complementary tool for HL-LHC crab-cavities operating with round optics, and as a crucial ingredient to boost the the performance of flat optics without crab-cavities.

Another remarkable conclusion in [9] is that the change of the tele-indexes of the x-y planes will not affect neither the optimal longitudinal and transverse position nor the optimal current of the wires. This makes the wires compensation naturally compatible with the β^*-levelling.

The objective of the MD program of 2017 was to demonstrate using the LHC wire prototypes the beneficial effect of the wire on the lifetime of Beam 2 when dominated by the LR detrimental effect.

The rationale of the MD is schematically reported in Figure 4. The idea is to have two (or more) bunches in Beam 2: one experiencing HO and no LR (that we will call super-PACMAN, see [2]) and a second experiencing HO and LRs (regular bunch). The most adequate observable for our scope are the losses normalized to the instantaneous luminosity, that corresponds to the so called effective cross section, σ^i_{eff}, of the i-th bunch of Beam 2:

$$\sigma^i_{eff} = -\frac{1}{\sum_{IPs} L^i_{IP}(t)} \frac{dN_i(t)}{dt} \tag{1}$$

where L^i_{IP} represent the instantaneous luminosity at the generic IP of the i-th bunch of Beam 2 (and Beam 1) and $N_i(t)$ is the bunch population of the i-th bunch of Beam 2.

In the ideal case (absence of LR), the experimental evidence shows that the $\sigma_{eff} \approx$ 80 mbarn, which corresponds to the total inelastic proton cross-section at 6.5 TeV.

During the MD three different phases can be envisaged:

1. burn-off dominated, where the LR detrimental effect is absent or negligible and therefore $\sigma_{eff} \approx 80$ mbarn.

2. LR dominated, where the LR detrimental effect (for the bunch experiencing it) is increasing significantly the σ_{eff} ($\sigma_{eff} >> 80$ mbarn). This effect is in general a transient effect (see transient decay in Figure 4).

3. LR compensated, where the wire compensation alleviate the LR effect allowing the σ_{eff} to recover its burn-off dominated value ($\sigma_{eff} \approx 80$ mbarn). The main objective of the MD is to evaluate the σ_{eff} after compensation of the regular and super-PACMAN bunch. A good compensation is achieved when both σ_{eff} are close to the 80 mbarn.

As shown in Figure 4, the σ_{eff} is a metric for the luminosity burn-off efficiency: following our approach $\sigma_{eff} = 80$ mbarn corresponds to 100% burn-off efficiency (all protons lost in Beam 2 are luminosity burnt-off) whilst $\sigma_{eff} = 160$ mbarn corresponds to 50% burn-off efficiency (only half of the protons lost in Beam 2 are luminosity burnt-off, the other half is lost, under the hypothesis of ideal collimation efficiency, in IR3 and IR7).

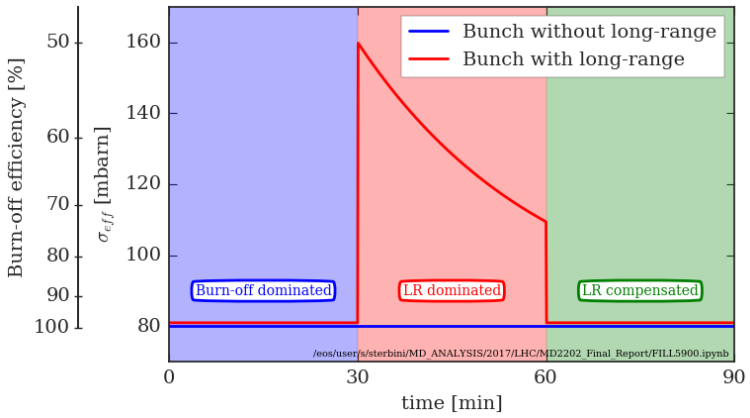

Figure 4: A schematic simplification of the rationale of the MD.

As it will appear clear in the following, due to machine protection constraint, the Beam 2 has to operate within the SAFE BEAM intensity limit ($I_{Beam2} < 3\ 10^{11}$ p). This means that nominal bunch trains in Beam 2 are excluded and only few bunches can be considered. Indeed several pilot bunches (PILOT) could be injected but in order not to weaken too much the losses signal (and therefore the Signal to Noise Ratio, SNR, for our observables, see Equation 1), we considered only nominal bunch range of intensity (i.e., $0.9 - 1.5\ 10^{11}$ p).

In the following we will present in two separate sections the results of the MD of the 1st July 2017 and 29th November 2017. The 2 h allocated for MD 2202 on the 17 September 2017 (originally a 9 h-slot was scheduled) will not be reported since, due to the unavailability of the machine (quench protection problem and cryogenic condition loss), no measurement could be performed.

1.2 Dimensioning of the wire compensation

From the theory in [9] and given the particular optics of the LHC one can compute the optimal longitudinal position (s_W), beam-wire distance (d_W) and current (I_W) of the wires. The wires have

- to be positioned at 158 m from the IP.
- To mimic N_W=19.28 encounters ($\int I_W dl = N_W \times c \times q \approx 110$ Am).
- To be at a distance of 5.66 mm from the beam ($\approx 7.5\ \sigma_{coll}$ at the right wire of IR5). This quantity scales linearly with the θ_c and the reported value holds for $\theta_c = 150\mu$rad.

Due to integration constraints, the wires where installed at about 150 m from the IP (see Figure 5) and the minimum reachable d_W is constrained to values in the range of 7-8 mm (jaws from 6 down to 5 σ_{coll}).

Since the parameter of the ideal compensation could not be achieved, it was decided to explore a scenario with maximum current $I_W = 350$ A and beam wire-distance of the left (d_{WL}) and right (d_{WR}) wire different and equivalent to 6 or 5.5 σ_{coll} (that is as close as possible without modifying the settings of the primaries collimators). This cannot provide a full RDT compensation but only a partial one.

In Figure 6 the horizontal and vertical IR5 bumps with respect to the reference orbit are shown (the vertical bump to lower the IP5 vertical position by 1.5 mm is clearly visible).

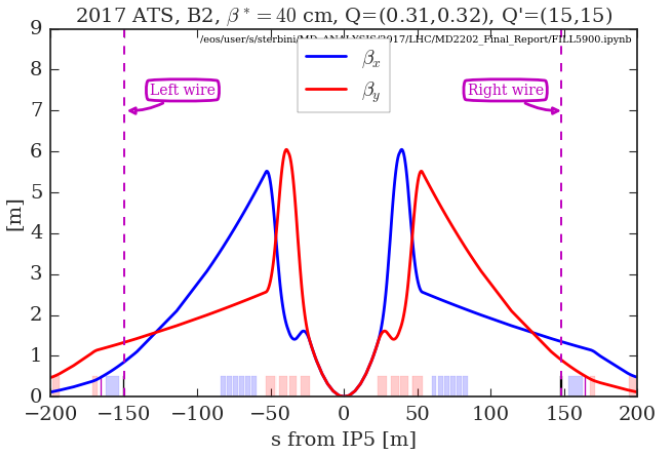

Figure 5: Beam 2 optics in IR5.

2 MD on 1st July 2017

The optics used during this MD was ATS 2017 with $\beta^* = 40$ cm. We had 2 fills: the 5898 and the 5900 (Figure 7). An analytical summary of the MD is shown in Figure 8.

The FILL 5898 ended prematurely due to a dump induced by a RF interlock. The RF expert could not determine the root cause of the dump since of the data of the post-mortem

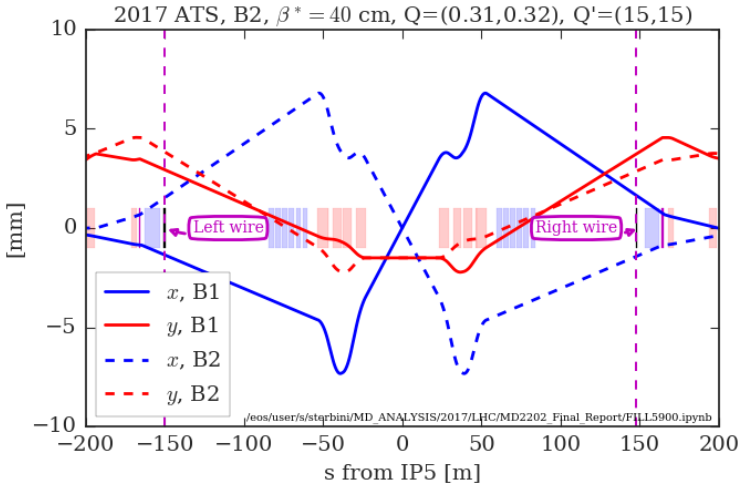

Figure 6: Horizontal and vertical orbit in IR5 (relative to the reference orbit).

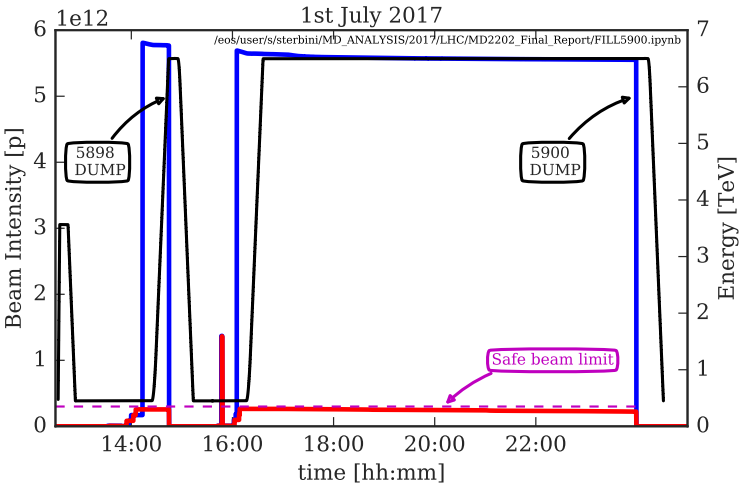

Figure 7: Fills in the MD of the 1st July 2017. Only during FILL 5900 relevant measurement could be carried out.

were all negative: probably it was due to a glitch of the RF interlock itself. The dump occurred almost at the end of the ramp-up. This acceleration was performed with half-detuning. The Engineer in Charge, after discussions with the RF Piquet, decided to perform the FILL 5900 ramp will with full detuning. In the following analysis we will consider only the FILL 5900 since no measurement could be carried out during the FILL 5898.

To be noted that the previous MD (MD2183) ended 1 h ahead of the schedule. This allowed E. Effinger to perform a fast access in order to recable the diamond BLM (dBLM) electronics to make it available for Beam 2. Since YETS17-18 both beams have a dedicated dBLM acquisition electronics.

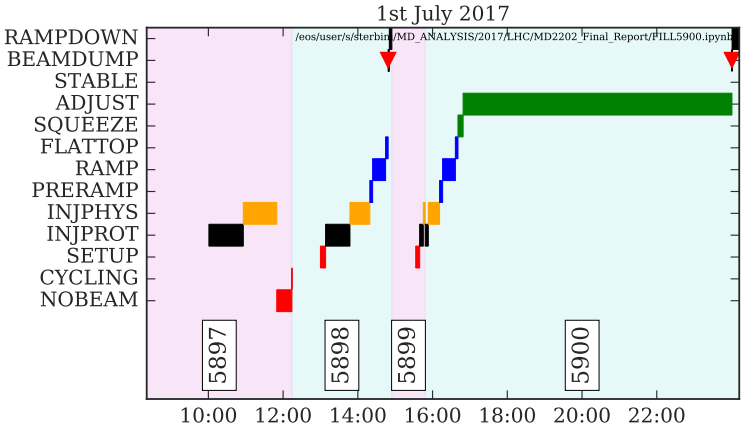

Figure 8: Analytical summary of the 1st July 2017 MD.

2.1 Filling scheme

The filling scheme used for the MD is summarized in Figure 9.

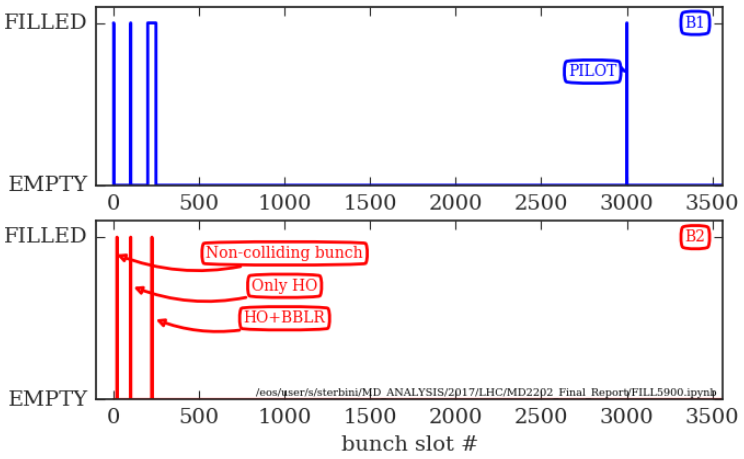

Figure 9: Filling scheme used for the 1st July 2017 MD.

It is worth noting that, differently of the simplified case presented in Figure 4, 3 bunches are injected in Beam 2. One of the three will serve to measure the tune (no HO, no LR collisions). The train of the Beam 1 is a standard BCMS train (48 bunches). Therefore the bunch of Beam 2 meeting the Beam 1 train will experienced 1 HO and 47 LRs (not equally distributed on the left and on the right of the IP1/5). No collision will occur in IP2/8 (see Figure 58). A more detailed description of the BB encounter schedule in IR5 (and for symmetry IR1) can be found in Figure 59.

2.2 Alignment of the wires

The Collimation Team provided the support during the MD for aligning vertically the wires with respect to Beam 2. This is not a trivial procedure since the pick-up, PU, of the collimator are placed in the horizontal plane. The vertical alignment can be done by scanning the vertical position of the wires and find the maximum induced sum signal on the PUs (positioned upstream and downstream the collimator's jaw). This assumes that the PU and the wires are vertically aligned (by design). A posteriori one can verify that that the vertical alignment is correct by measuring the vertical kick given by the wire when powered. To ease this test the orbit feedback has to be switched off.

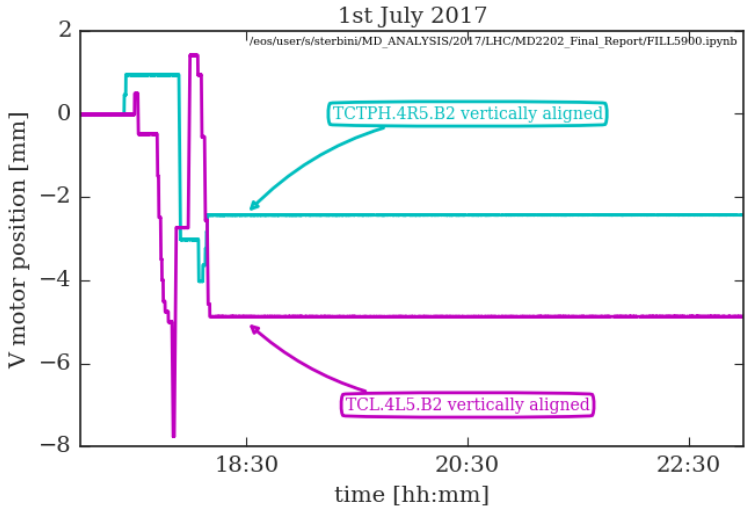

Figure 10: Vertical alignment of the two collimators (5^{th} axis).

In Figure 10 the procedure of the alignment of the vertical axis (the so called 5^{th} axis) is showed. It is worth noting that the Δy is significant (almost -5 mm on the left wire). This has to be compared with the full gap aperture of the collimator shown in Figure 11 and corresponding to less that 10 mm.

For the sake of completeness, the movement of the 4 axes in the H-plane of the two collimators is reported in Figure 12. Particular attention was payed to align the beam in the center of the downstream and upstream PU for the H-plane. A similar procedure was not possible for the V-plane since only one axis was available (5-th axis): an average alignment was therefore performed.

In addition to the wire collimators and following the Machine Protection Panel recommendation, the asynchronous dump aperture protection (TCSP) was moved and positioned to 5.5 σ_{coll}, that is 0.5 σ_{coll} lower than the wire collimator's jaws (see Figure 60 in Appendix B).

2.3 The bunch-by-bunch intensity

In this paragraph we are going to present the bunch-by-bunch intensity evolution along the fill. In Figure 13 the evolution of the Beam 2 bunch intensity is shown. It is worth observing

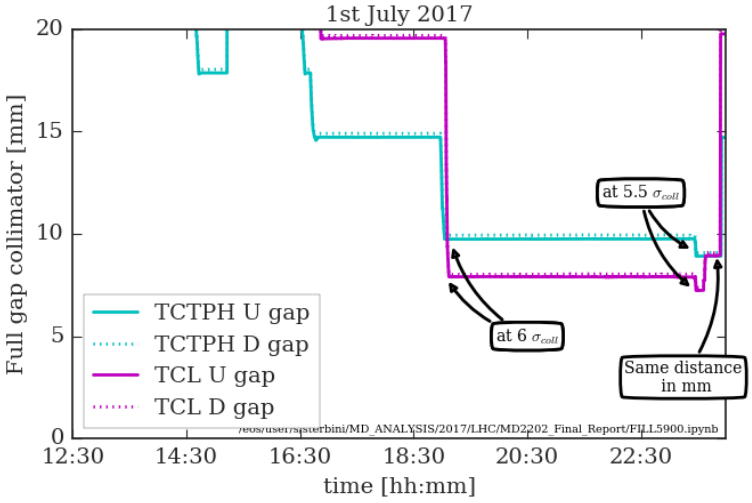

Figure 11: Horizontal alignment of the two collimators.

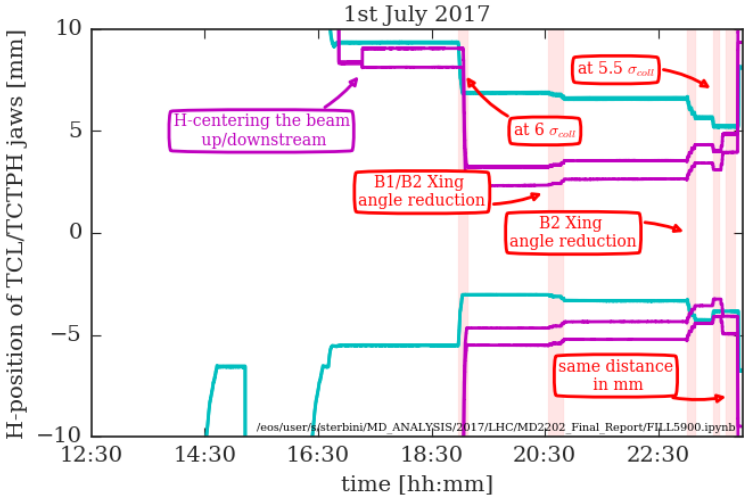

Figure 12: Horizontal alignment of the two collimators with the 4 axes.

that the bunch without collision (#20) did not experienced losses, this is not the case for the bunches with HO (#100 and #224) and with LR (#224). The losses around 18h40 and 21h00 are due, see Section 2.4, to the controlled blow-up induced by the damper (ADT).

In Figure 14 the evolution of the Beam 1 single bunch intensity is shown. Even if the blow-up of Beam 2 bunches will induce, via the HO collision, a blow-up in Beam 1, the losses on Beam 1 (namely on #100) are not observable on the scale of the plot.

It is interesting to observe the evolution of the intensity of the bunches of the Beam 1 train (Figure 15). It is clearly visible the instability of the bunches without HO. This a typical feature of the asymmetric filling pattern. We tried to stabilize Beam 1 by increasing the octupoles current (see Figure 61 in Appendix B).

In addition to the instability on Beam 1, there was a RF problem in Beam 2 that causes

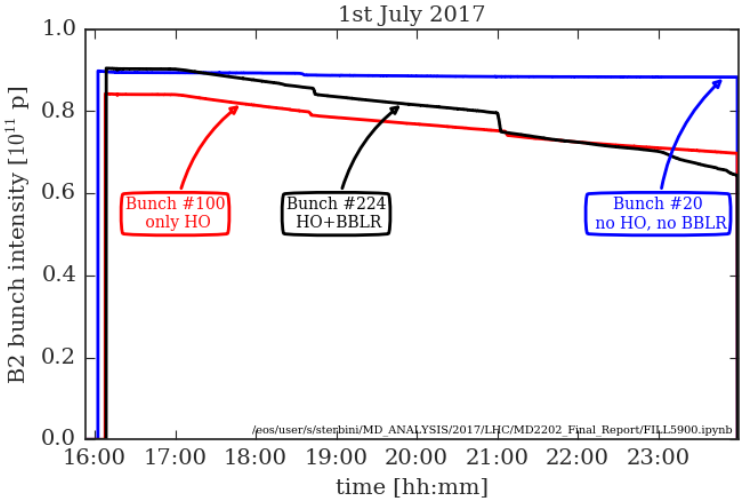

Figure 13: Evolution of the bunch-by-bunch (bbb) intensity in Beam 2.

a violent blow-up (BU) in the longitudinal plane (see Figure 62 in Appendix B). Fortunately the Beam 2 was defined as SAVE BEAM and that automatically masked the corresponding RF interlock. The instability on transverse plane in Beam 1 and the longitudinal plane in Beam 2 was not considered a problem for the second part of the MD.

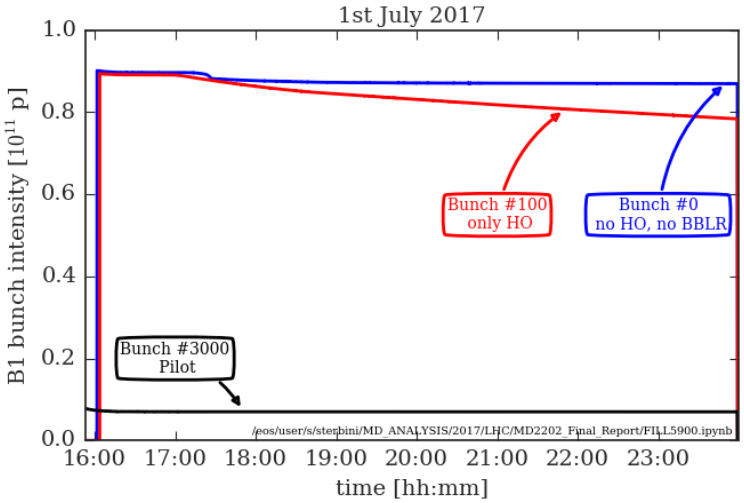

Figure 14: Evolution of the bbb intensity in Beam 1 (only three bunches are shown).

2.4 Controlled transverse blow-up of Beam 2

Past and recent operational observations and machine development sessions showed a clear asymmetry between Beam 1 and Beam 2 lifetime: Beam 2 lifetime is in general better (higher lifetime) than the one of Beam 1. The reason of this observation remains obscure even if

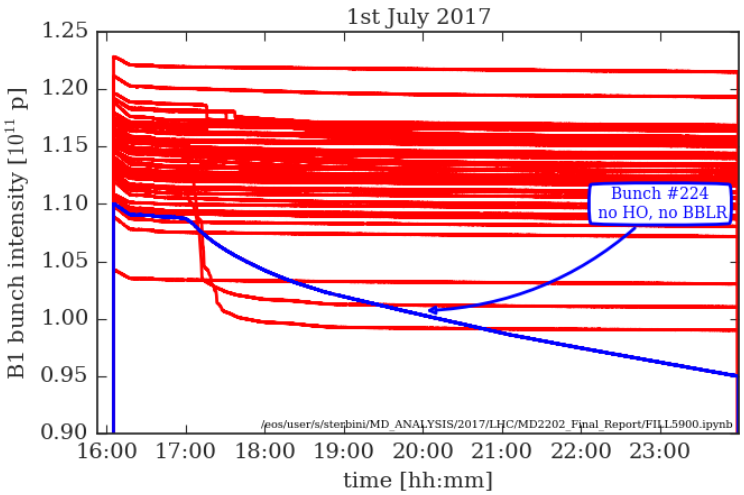

Figure 15: Evolution of the bbb intensity in Beam 1 (bunches in the train).

several educated hypotheses have been formulated. As mentioned in Figure 4, in order to compensate the effect of LR one has to observe a clear signature of the problem. This for Beam 2 can be a limiting factor. In our case we enhance the LR effect on Beam 2 with a two-fold strategy:

1. tail re-population via controlled blow-up (H-plane),

2. reduction of the crossing angle to increase the LR.

The latter solution has the drawback to increase the complexity of the correction (reducing the crossing angle implies the need to reduce the beam-wire distance, that is presently limited by the prototype design). Our privileged strategy is therefore to re-populate the beam tails via a bunch-gated excitation of the ADT (H-plane).

We can see in Figure 16 the time windows where the ADT Beam 2 H-plane was active. The corresponding losses in the bunches can be observed in Figure 13.

The corresponding blow-up of the Beam 2 bunch sizes can be observed from the BSRT reading (Figure 18). One can clearly see horizontal (and vertical) blow up between 18h and 19h and around 21h.

A vertical instability was triggered on bunch #20 when approaching the diagonal and, crossing the diagonal produced an emittance exchange of the bunch #100 and #224 (no instability, possibly due to the HO collision).

From 21h30 and 23h30 as we will see the wires were powered (Section 2.6) and this induced a visible $\approx 10\%$ β-beating (see Figure 18).

2.5 The crossing angle reduction

The crossing angle in IP1 and IP5 was reduced by steps as shown in Figure 19. One can observe two different main trims:

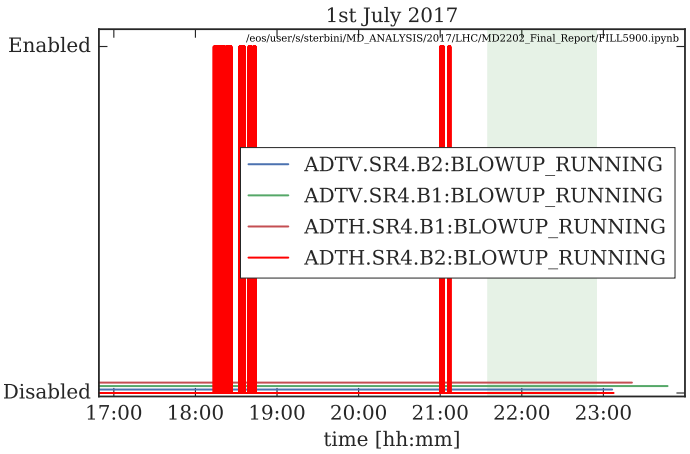

Figure 16: ADT blow-up.

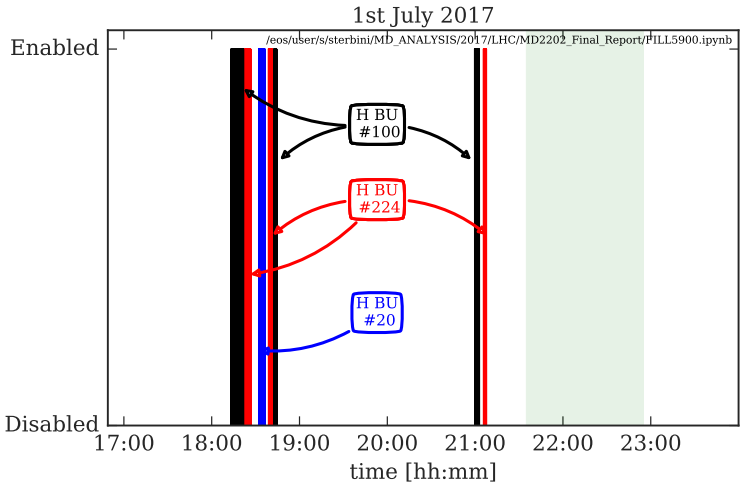

Figure 17: ADT blow-up with gating windows.

1. the one around 21h40: it was done by the standard crossing angle knobs in steps of $-5, -5, -10$ and -10 μrad,

2. the one around 23h00 when only the angle of the Beam 2 at the IP1 and IP5 was modified in 4 steps of -10 μrad, for a total of -20 μrad of half-crossing angle. The purpose of this second trim was to test the new knobs and eventually to balance the lifetime between Beam 1 and Beam 2. In this condition (half-crossing angle of 100 μrad), as already mentioned, the wire compensation will be very difficult to achieve. This is mainly due to the constraint on the distance between the beam and the wire imposed by the position of the wire collimator jaw (at 6 σ_{coll} from the beam).

It is worth noting that due to limits of the orchestration at the time of the MD (presently this limit has been removed), the IP1 and IP5 crossing angle variations were performed with

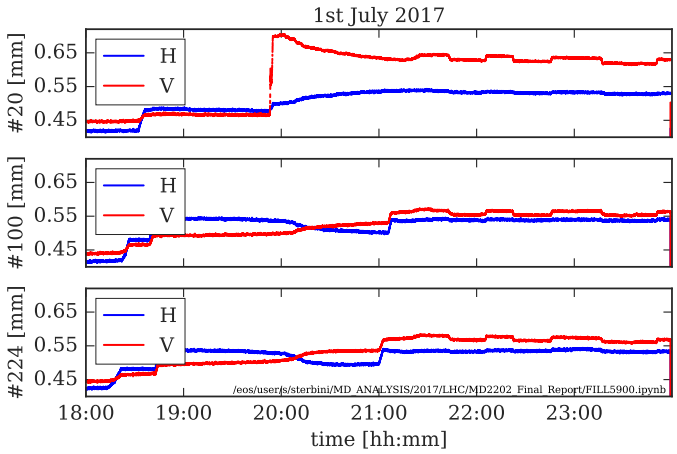

Figure 18: BSRT reading for the beam size of the three bunches of Beam 2 (in sigmas).

a slight delay.

The IP2 half-crossing angle (V-plane) during the measurement was maintained to 200 μrad and the IP8 half-crossing angle (H-plane) to -250 μrad. During the full MD and especially when changing the crossing angles, attention was paid in re-optimizing the luminosity via standard luminosity scans. For the sake of completeness we report them in Figures 63 and 64.

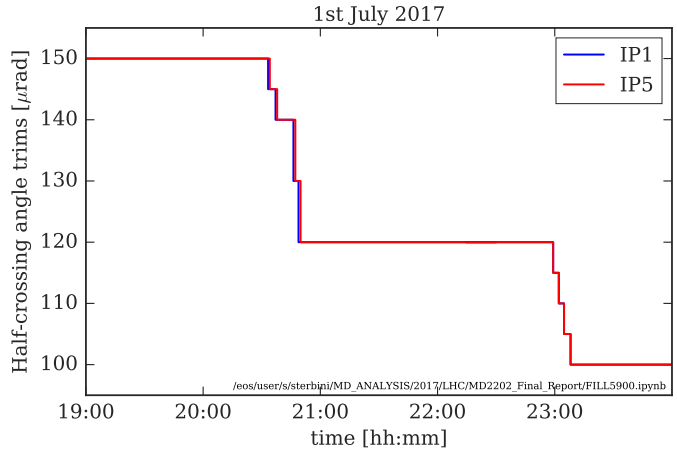

Figure 19: Half-crossing angle reduction in IP1 and IP5.

2.6 The powering of the wires

Finally the wires were powered as shown in Figure 20. We started by powering the right wire and with a very gentle ramp rate. The wires excite an infinite number of multipoles: the dipolar and quadrupolar ones have to be corrected since they would change the orbit and the

tunes of the beam making impossible a direct comparison before and after the compensation. We will refer to these automatic corrections as feed-forwards.

During this MD a manual correction was put in place. Each time ones or both wires were trimmed, a convenient trim with the same ramp rate was programmed on the Q-trim quadrupoles and on the dipole correctors close-by the wires. In doing so the orbit effect of the wire was locally corrected but the quadrupolar effect, due to the non-local correction, produced the β-beating observed in Figure 18. This approach was improved significantly in the MD of the 29th November 2017 when the procedure was automatized and the quadrupolar feed-forward used close-by quadrupoles (local correction, special thanks to G.-H. Hemelsoet and M. Solfaroli). The performed Q-trim and corrector trims are shown respectively in Figures 21 and 22. It is worth noting that (Figure 21), some minor adjustment on the Q-trims were needed to compensate the machine drift and/or the limited accuracy of the wires modeling. The trims of the converters RCBYHS4.R5B2 and RCBYHS4.L5B2 (Figure 22) are the sums of the the feed-forward trims, the closed-orbit (CO) feedback, the crossing angle trims and the luminosity scans.

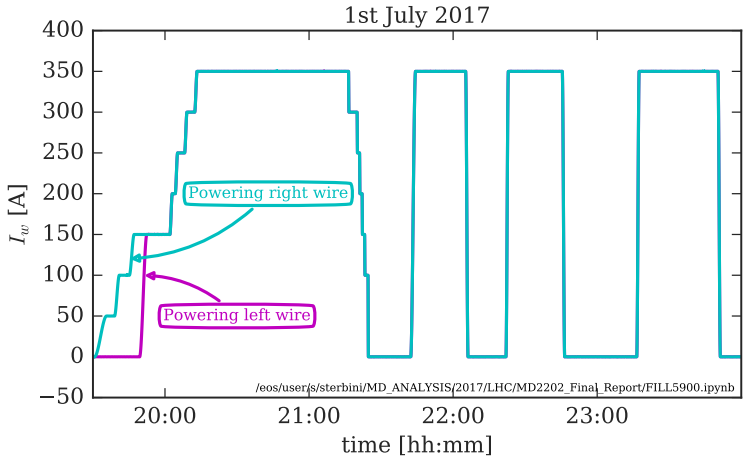

Figure 20: Powering of the right and left wires.

For the sake of completeness we show the status of the tune feedback, CO feedback and energy feedback respectively in Figures 65, 66 and 67. During the compensation in general we worked with the tune feedback switched off and the CO and energy feedback switched on.

It is interesting to verify the stability of the orbit at the wire collimators (Figure 23). Thanks to the feedforward and to the CO feedback the stability of the orbit is at the level of 10 μm or better. Some of the spikes are due to the luminosity scans.

To verify the vertical alignment of the wire one can check the stability of the vertical orbit of the beam. In Figure 24 we showed the PU readings of the TCTPV close to the right wire. This test shows a very good stability of the optics but cannot be considered fully conclusive since the CO feedback is on.

A more detailed analysis of the CO feedback signals are reported in Appendix A.

It is interesting to verify the stability of the tune during the powering cycle of the wires.

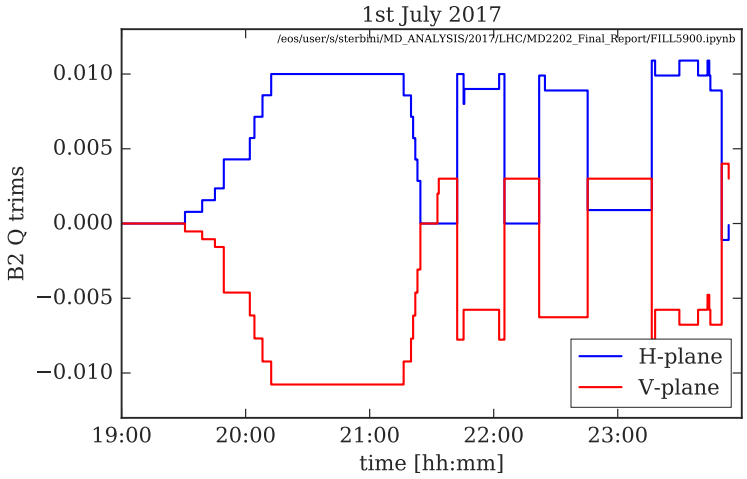

Figure 21: Q-trims of Beam 2.

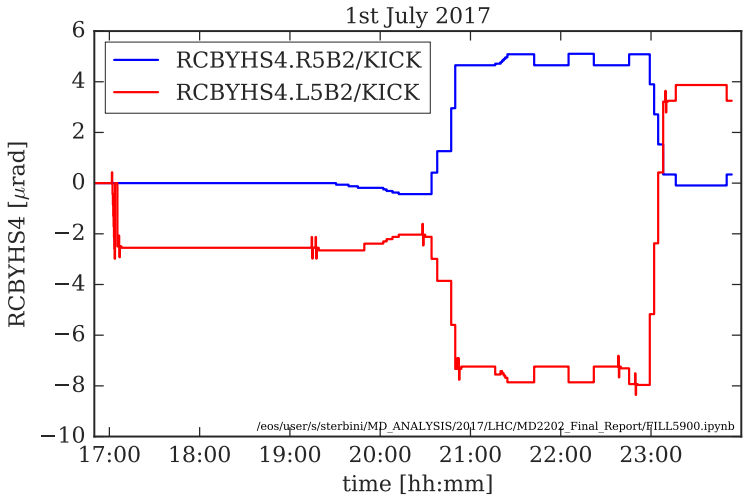

Figure 22: Corrector trims of Beam 2.

The results is reported in Figure 25. With the exceptions of the offsets around 21h40 and 22h00 (due to the limited accuracy of the quadrupolar response of the wire) the tune stability is very good. One can also appreciate that during the second power cycle (from 22h15 to 22h55), the tune feed-forward was significantly improved. It is worth stressing the importance of the tune stability: from simulation (see for instance [**?**]) and experimental evidence, the lifetime of the beam is affected by trimming the tune at the 10^{-3} level. For our MD is therefore crucial to control the tune with great accuracy to disentangle the effect of the non-linear RDT compensation of the wire from the effect of a simple tune trim.

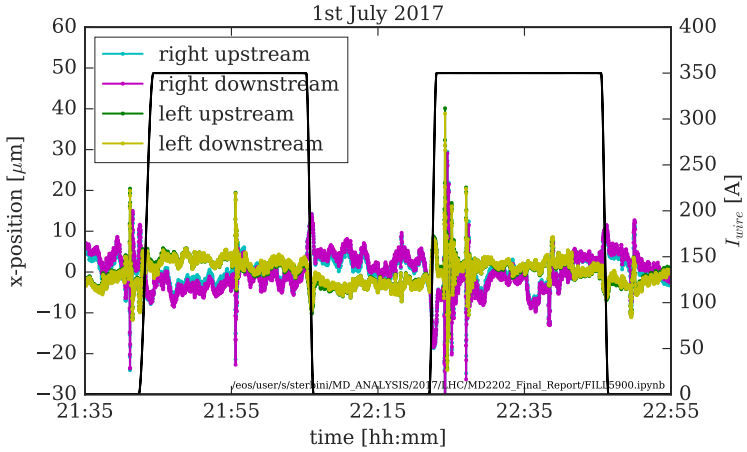

Figure 23: Orbit stability (H-plane) at the wire collimator during the powering of the wires.

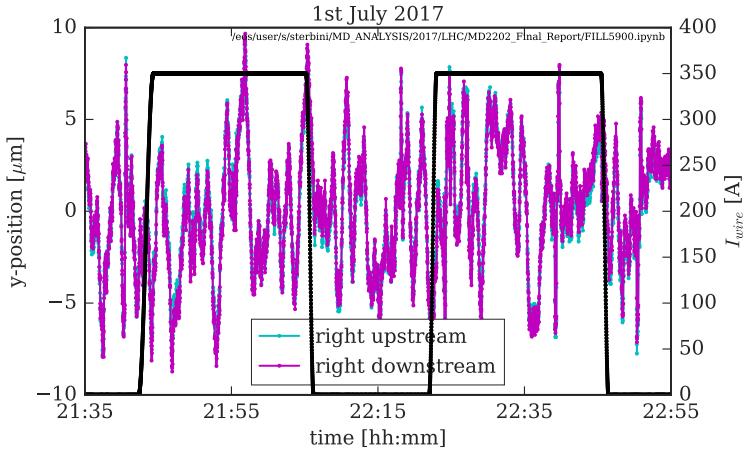

Figure 24: Orbit stability (V-plane) at the TCTPV close to the right wire during the powering of the wires.

2.7 The hardware checks

During this first MD, special attention was devoted to the behavior of the hardware and to ensure its correct functioning. A constant scrutiny of the power converters was put in place checking the different states of the devices as shown in Figures 68 and 69.

In addition to the power converter the temperature of the jaws of the wire collimator were constantly monitored (see Figures 26 and 27). One can observe that in normal operation the variation of temperature of the jaw due to the wire is less than 10 degrees and the margin to the temperature limit of the collimator is relatively large.

As requested by the Machine Protection Panel, before powering the wires, tests of the HW interlock were performed. The HW interlock monitors the voltage on the wires. If the voltage overtakes the $V_{thres} = 2.9$ V (that is there are anomalies on the current of the wire

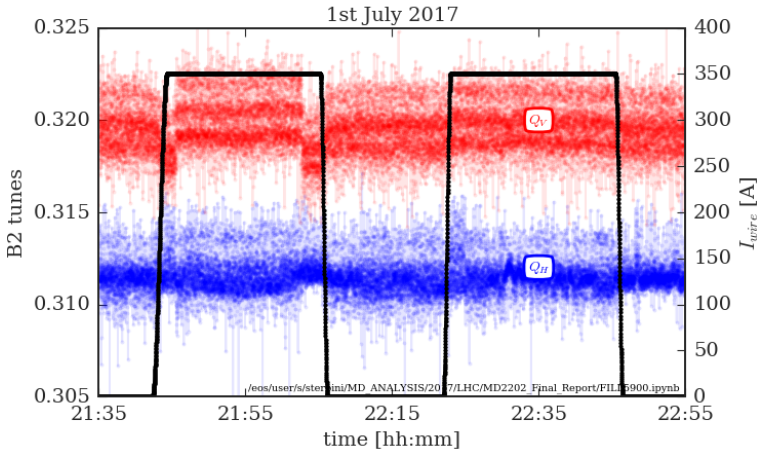

Figure 25: Tune stability during the powering of the wires.

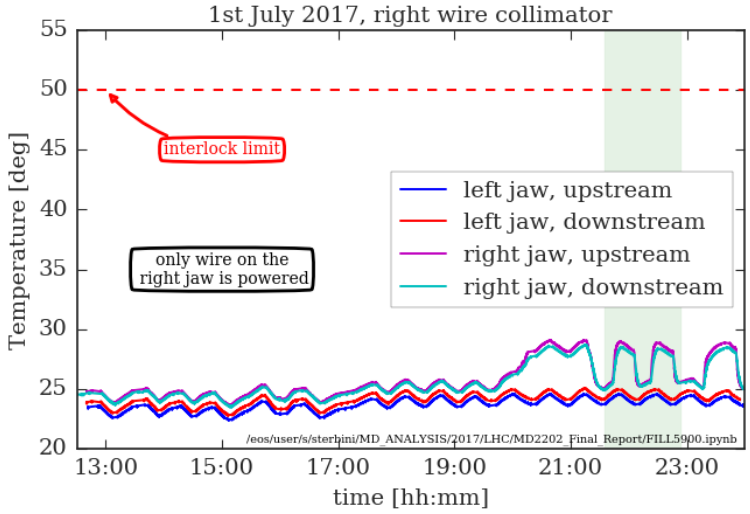

Figure 26: Temperature of the right wire collimator.

and/or its temperature) the interlock is triggered. The interlock test is done by lowering V_{thres} to 0 V and by verifying that the interlock behaves as expected.

The results of the test are reported in Appendix B. There are four different V_{thres} respectively for the internal/external left wires and the internal/external right wires (Figures 70, 71, 72 and 73). The voltage on the wires was also monitored (see Figures 75 and 76). A comfortable margin with respect to the $V_{thres} = 2.9$ V used for the the HW interlock was observed.

The vacuum level close to the wire location was also monitored (see Figure 74). No issues were observed in that respect.

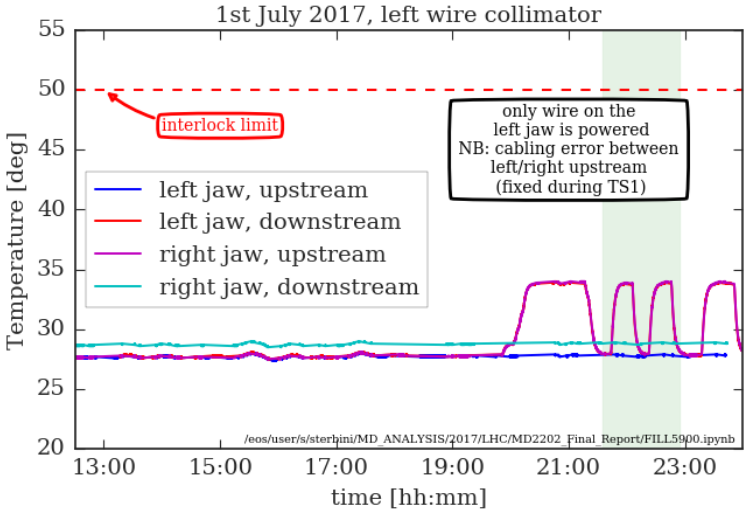

Figure 27: Temperature of the left wire collimator. To note the cabling error between the temperature sensors of the right and left jaw downstream. It was fixed after the MD.

2.8 The efficiency of the compensation

In this section we analyze the efficiency of the compensation. Different approaches can be envisaged. The most straightforward is to consider the effective cross-section, σ_{eff}, as explained in Section 1.1. This is presented in Figure 28. When switching off the compensation an increase on the σ_{eff} is visible whilst the effect on the super-PACMAN (suffering only HO) is modest. A similar information can be represented by normalizing our ideal effective cross-section (80 mbarn) with respect to σ_{eff} (see Figure 29).

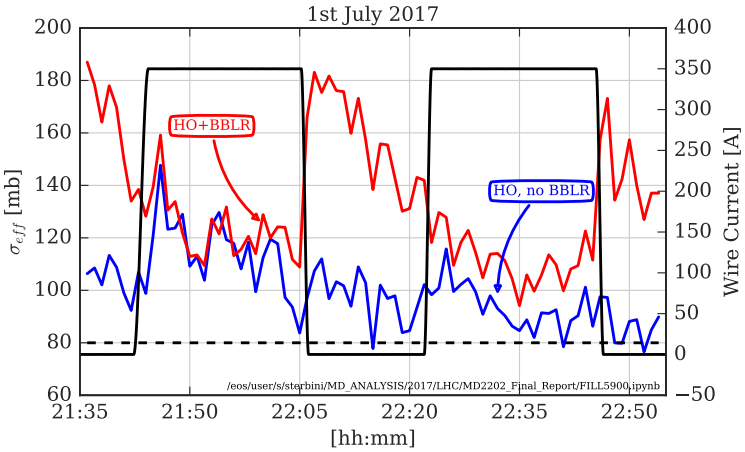

Figure 28: Effective cross-section of the Beam 2 bunches with and without compensation.

A complementary way to show the effect of the compensation is to compare the lifetime of the bunches of Beam 2 (see Figure 30). It is possible to observe that the lifetime of the

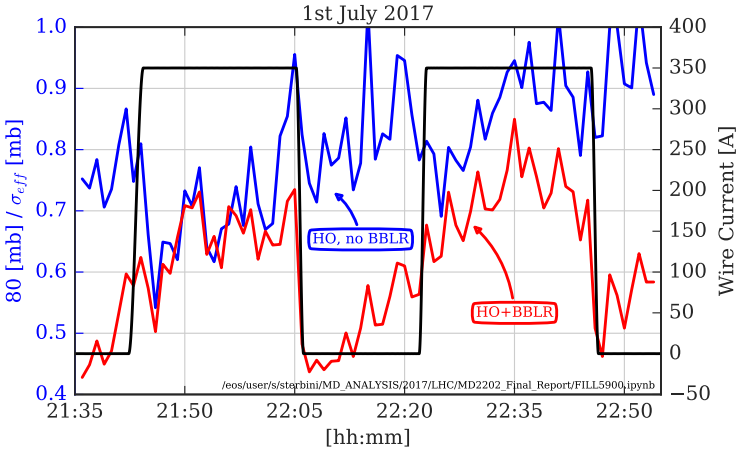

Figure 29: Normalized inverse of the cross-section of the Beam 2 bunches with and without compensation.

bunch with no LR is $\approx$ 45 h. The one of the bunch with LR varies between a minimum of $\approx$ 25 h without compensation to an average of $\approx$ 35 h with compensation. One can

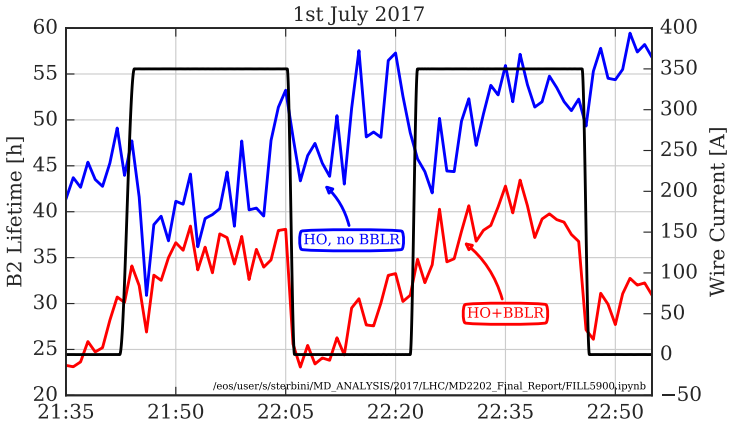

Figure 30: Lifetime of the Beam 2 bunches with and without compensation.

directly compare the losses (after having compensated the luminosity driven losses) of the two bunches (see Figure 31).

For all observables considered, it is visible the effect of the loss of compensation when the wires are switched off. The neat effect by switching them on is less evident. The interpretation of this phenomenon has to be linked to the nature itself of our observable, that is the loss of particles due to variation of dynamic aperture, DA, of the machine in presence of diffusion mechanisms.

1. A contraction of DA produces losses (wires off) due to the relative fast depletion of the tails of the beam distribution. Once the tail present in the area of the DA contraction

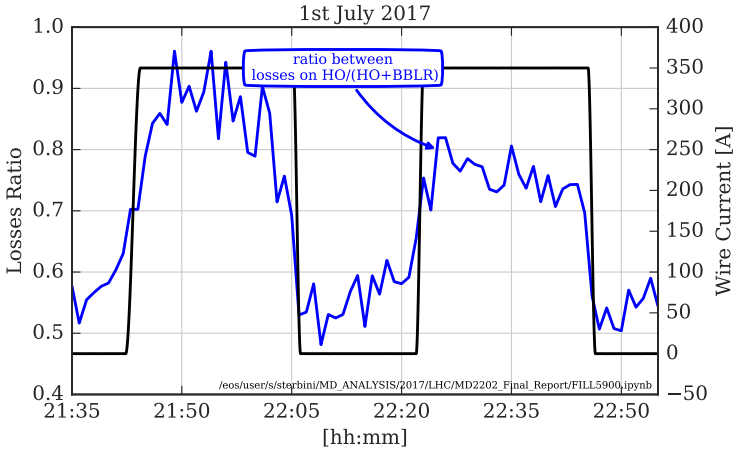

Figure 31: Losses ratio between super-PACMAN and regular bunches.

are depleted the new losses are possible only due a diffusive mechanism of the beam distribution. This mechanism is qualitatively in agreement with what is observed (transient and recovery of the lifetime).

2. When the DA increases, neglecting the diffusive mechanism, no effect on lifetime is expected. In our experiment is difficult to disentangle the effect of the switching on of the compensation and the natural re-population of the tails due to the diffusive mechanism.

The signals of the bunch-by-bunch lifetime is quite noisy: this is caused by the fact that this quantity is related to the derivative of the FBCT signals.

A significant effort was devoted in improving the SNR by measuring directly the bunch-by-bunch losses at the primary collimators. This would avoid the differentiation and measure directly the losses at the collimators. This approach is routinely used with the ionization chamber BLM (see B. Salvachua's presentation in [13]): one can convert linearly the BLM signals into beam losses (using the loss maps calibration signals). Unfortunately the ionization chamber BLM has not the bandwidth to resolve the bunch-by-bunch losses. Therefore one has to use faster BLM (the so called diamond BLM, dBLM). Due to significant data flow rate, event counting techniques are put in place based on a trigger threshold voltage. This in principle affects the linearity of the counts/losses relation. In Figure 32 we show the σ_{eff} computed starting from the dBLM (the calibration factor was computed by imposing a constraint on the average value of the σ_{eff}). Using dBLM data improved significantly the SNR (comparison between Figures 28 and 32). In the latter case one can appreciate also the tune trim correction (see Figure 25) and some of the spikes that are due to luminosity scans. In Figure 32 one can also start to appreciate the reduction of the σ_{eff} in the OFF/ON transition of the wire compensation.

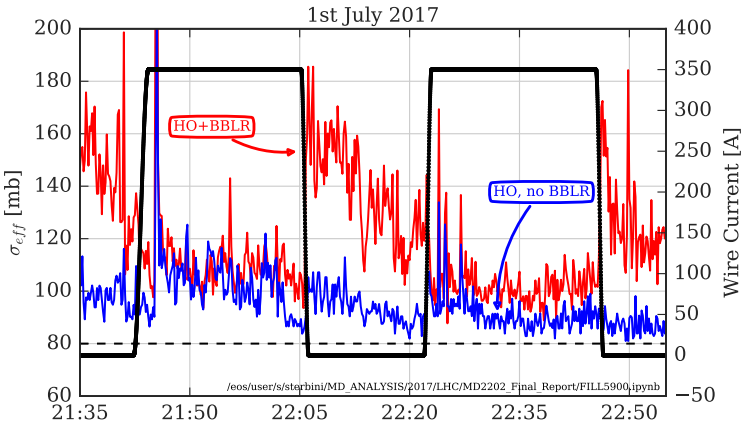

Figure 32: Effective cross-section of the Beam 2 bunches with and without compensation from dBML data.

3 MD on 29th November 2017

In this section we will report the results of the MD2202 of the 29th November (see Figure 33) putting emphasis on the difference with respect to the 1st July.

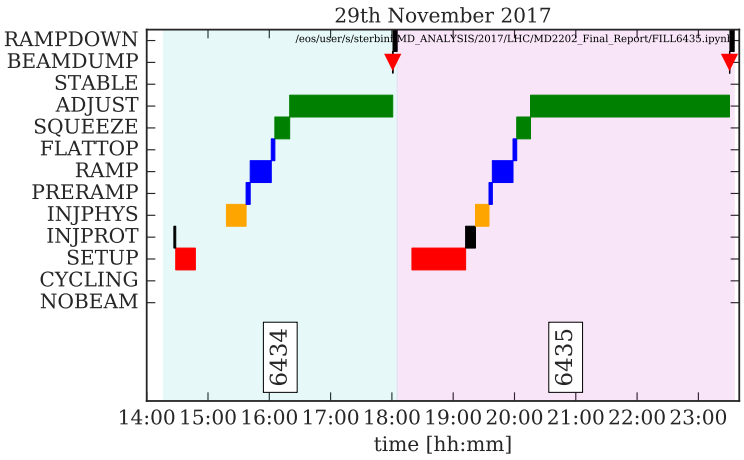

Figure 33: MD2202 of the 29th November.

On 29th November 2017, the setting of the wire collimators could be lowered from 6 σ_{coll} (see Section 2) to 5.5 σ_{coll} and this allowed to improve the correction efficiency.

The dipole and quadrupole feed-forwards were better integrated in the control system (special thanks to M. Solfaroli and G.-H. Hemelsoet). In particular the quadrupolar feed-forwards trimmed the Q4 and Q5 quadrupoles thus minimizing the β-beating. Unfortunately the interlock monitoring the current of this power supplies was not masked causing a dump (FILL 6434). In the following the data of the FILL 6435 are presented.

In FILL 6435 particular attention was devoted to the octupole configuration (Figure 34). To disentangle the effect of the wire compensators from the one of the octupoles, the Beam 2 octupoles were switched off after having put in collision the two beams. The Beam 1 octupoles were set to the maximum current to stabilize the strong beam (most of the bunches did not experienced HO collisions).

3.1 Filling scheme

The filling schemes for Beam 1 and Beam 2 is shown in Figure 35. The beam-beam encounters (HO and LR) occurred only in IP1 and IP5. Differently from the MD of the 1st July there were two instead of three bunches in Beam 2 (there was not the non colliding bunch for the tune measurement): we preferred this configuration to increase the current of the injected bunches. The total beam intensity is shown in Figure 36. In Figures 37 and 38 the bunch intensities of the relevant Beam 1 and Beam 2 are reported. The Beam 1 contains three trains and the regular bunch of Beam 2 is colliding with the third train: this configuration was chosen to reduce the probability of instability in the colliding train of Beam 1 (special thanks to E. Métral and L. Carver).

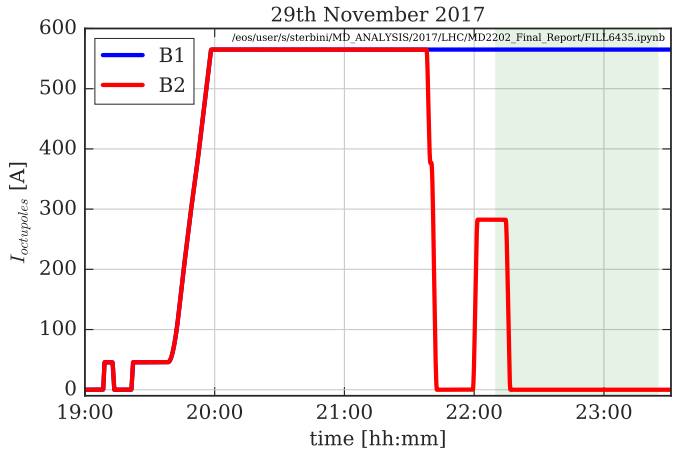

Figure 34: Octupoles settings.

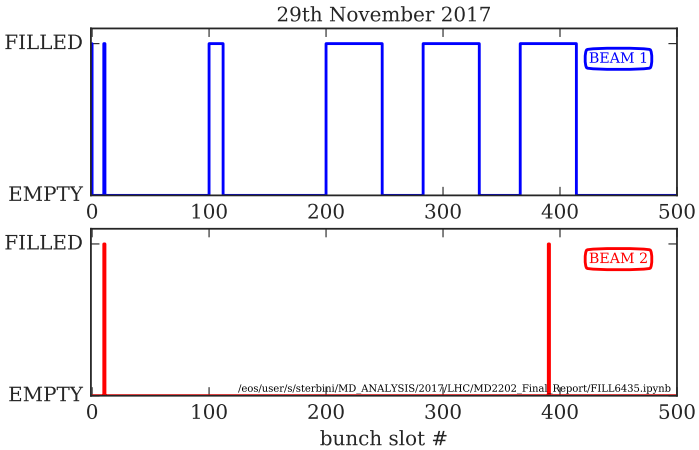

Figure 35: Filling scheme.

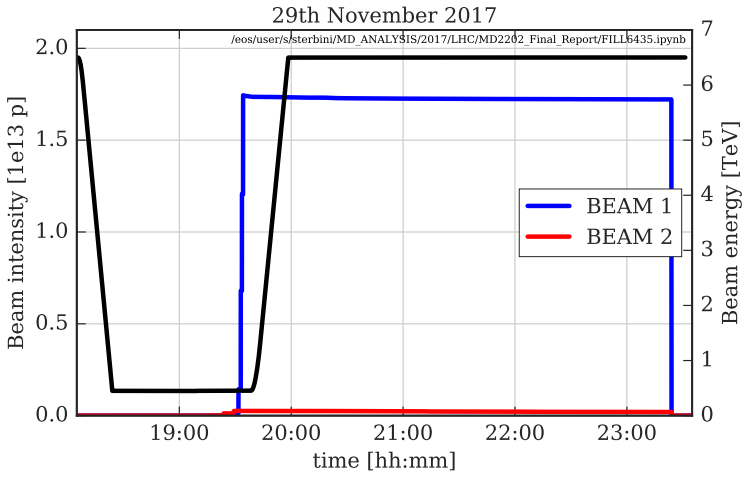

Figure 36: Total beam intensity.

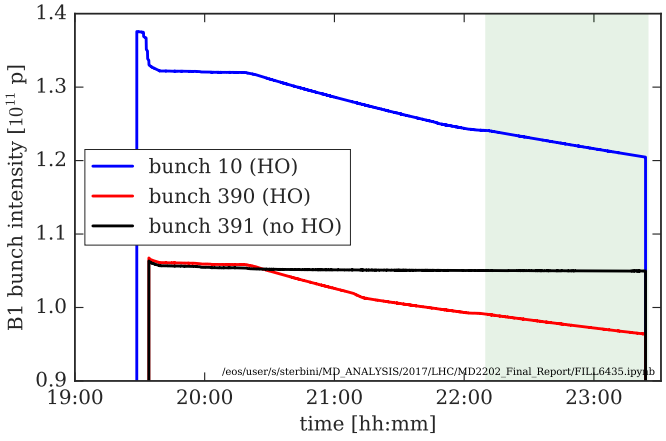

Figure 37: Intensity of bunches 10, 390 and 391 in Beam 1.

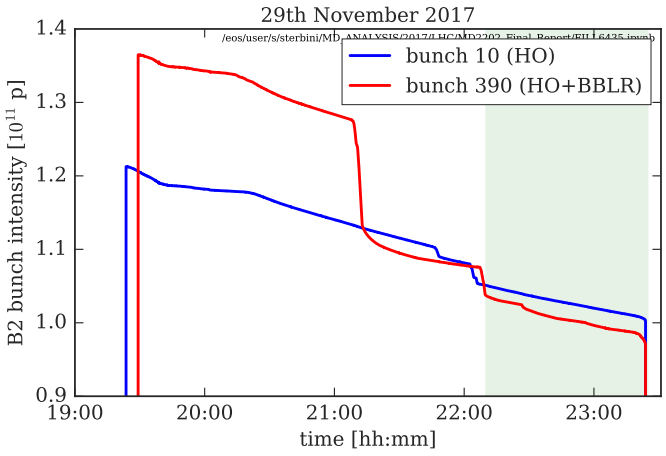

Figure 38: Intensity of bunches 10 and 390 in Beam 2.

3.2 Alignment of the wires

The alignment of the 5th axis was performed during the FILL 6434 and in the FILL 6435 the 5th-axis alignment was re-established a top energy using the FILL 6434 values (Figures 39 and 41). The half-gap of the wire-collimator was reduced to 5.5 σ_{coll} (Figure 40). As reques-

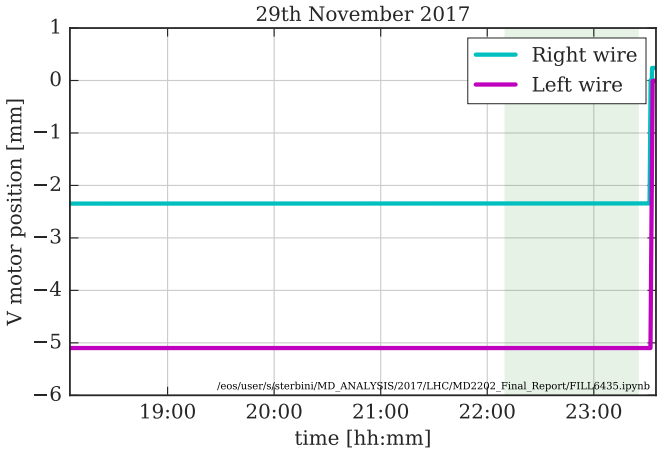

Figure 39: Wires vertical alignment (5-th axis).

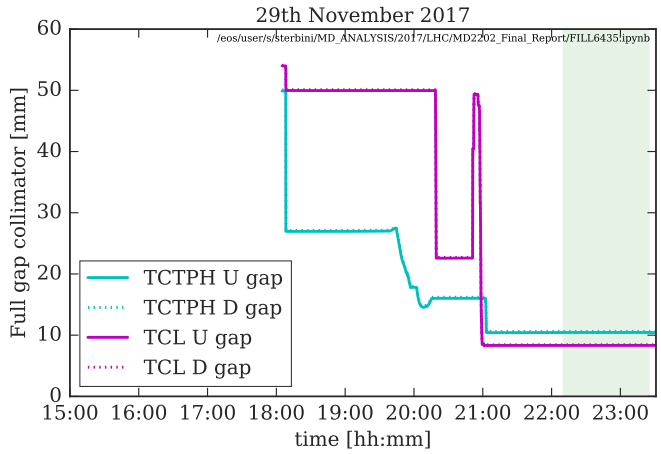

Figure 40: Wire-collimator horizontal gap.

ted by the Machine Protection Panel the TCSP half-gap was reduced to 5 σ_{coll} (Figure 60).

3.3 Controlled transverse blow-up of Beam 2

To establish a regime dominated by the beam-beam long range, the Beam 2 bunches were blew-up using the ADT excitation following a very similar approach of the one adopted during the 1st July MD. The only difference was to separate the Beam 1-Beam 2 during the

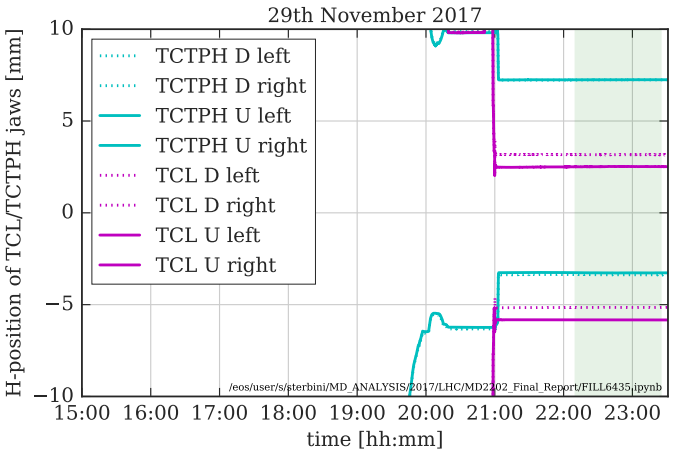

Figure 41: Wire-collimator horizontal jaws.

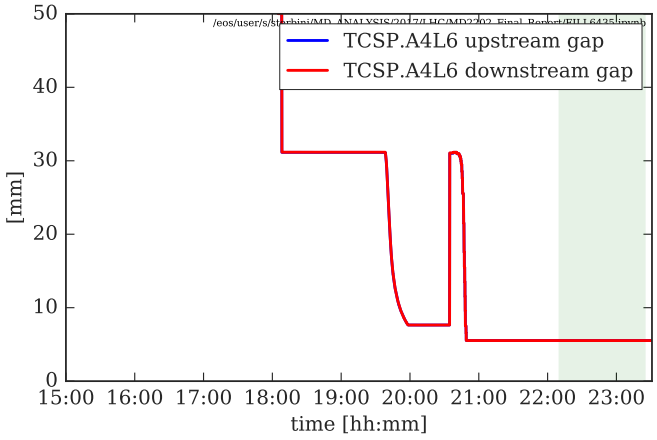

Figure 42: TCSP gap.

blow-up, in order not to blow-up the Beam 1 colliding bunches. During this procedure the octupoles of Beam 2 were increased (Figure 34, around 22h00) to guarantee a sufficient level of Landau damping.

3.4 Optics and crossing angle

The optics configuration of the MD was with $\beta^* = 30$ cm and $\theta_c = 150$ μrad as shown in Figures 43, 44 and 45.

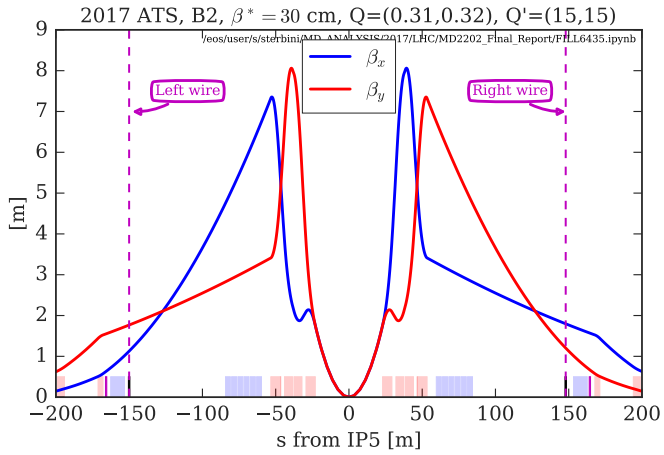

Figure 43: Beam 2 optics ($\beta^* = 30$ cm).

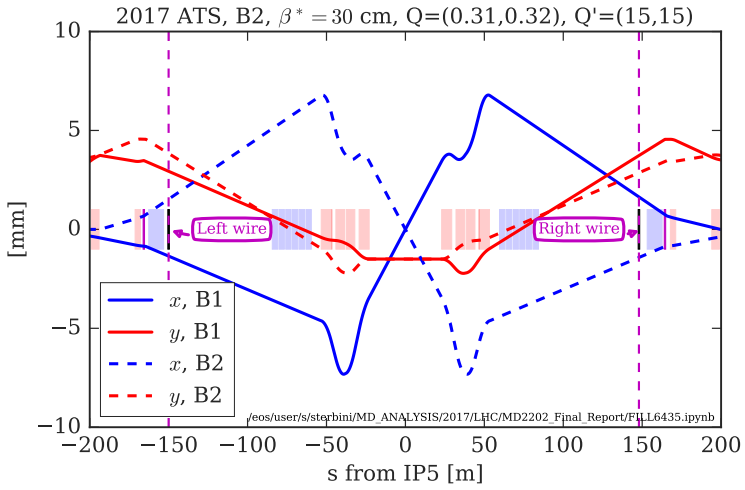

Figure 44: Crossing and separation bumps in IR5. During the MD the crossing angle was of 300 μrad. It is possible to see the -1.5 mm vertical bump of IP5.

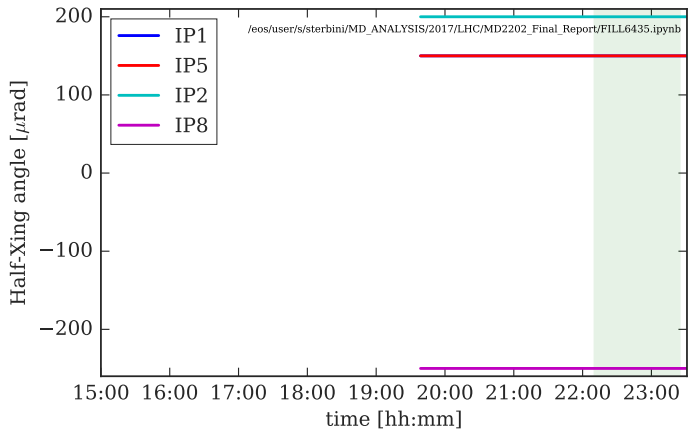

Figure 45: Crossing angles during the MD. The IP1 and IP5 operated with $\theta_c = 150$ μrad.

3.5 The powering of the wires

Using the approach suggested in [9], the current of the left and right wires was determined in order to minimize the (p1=0, q1=4) and (p2=4, q2=0) resonances (where the symbols follow the conventions in [9]).

The result of the numerical optimization is reported in Figure 46 where we consider the position of the jaw ranging between 4.5 and 5 σ_{coll}, that different beam-wire distance for the left and right wires. Given the jaw position of 5.5 σ_{coll} during the MD, the current was set to

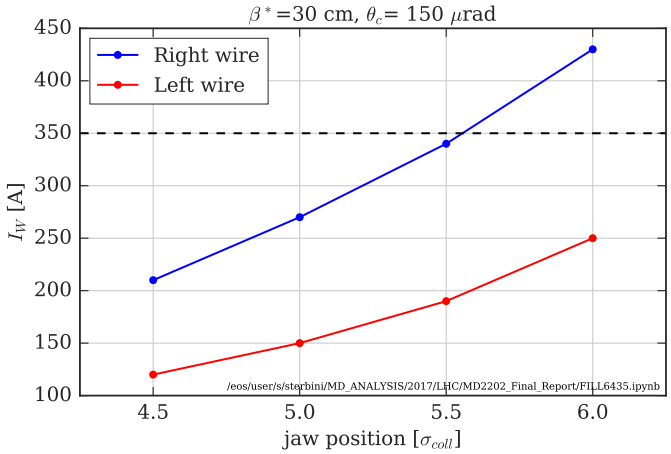

Figure 46: The powering of the wires.

190 and 340 A for the left and right wire, respectively (Figure 47). For completeness we show

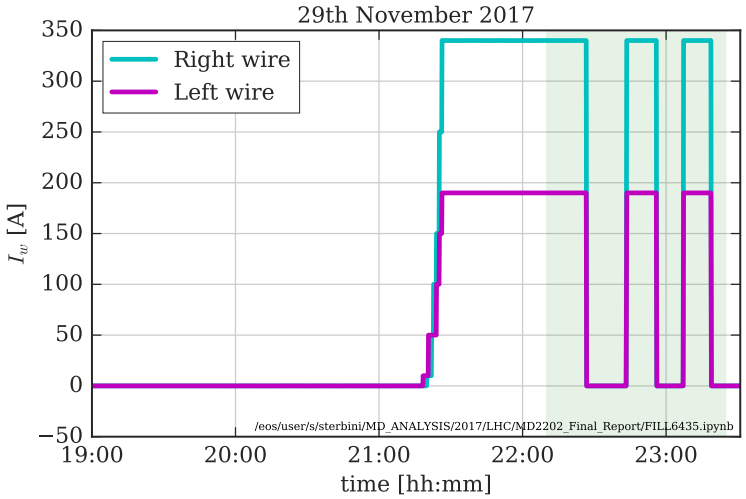

Figure 47: The powering of the wires.

in Figures 48 and 49 the effects of the dipolar and quadrupolar feed-forwards, respectively.

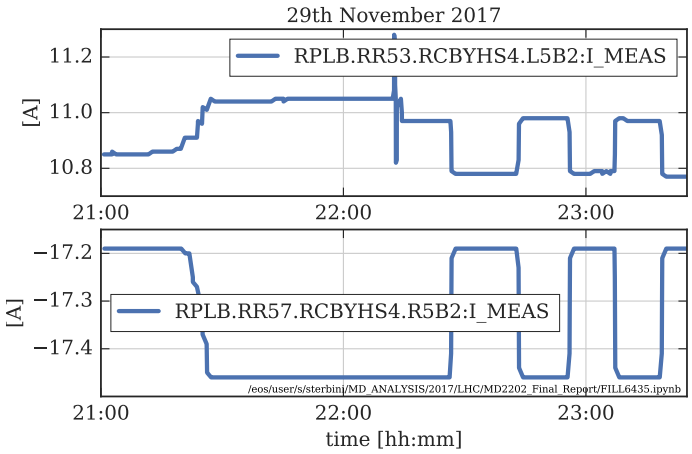

Figure 48: Dipolar feed-forward. The scan in current observed on the upper plot correspond to a luminosity scan.

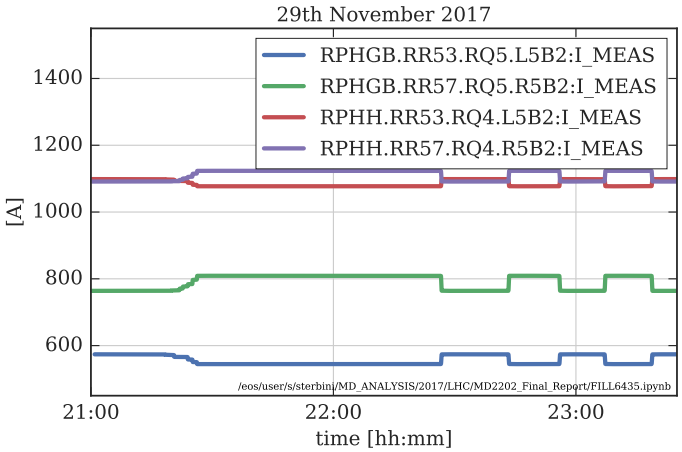

Figure 49: Quadrupolar feed-forward.

The effect of the horizontal and vertical CO stability during the wire powering is minor (≈ 50 μm, see Figures 50 and 51).

Due to the absence of a non-colliding beam in the Beam 2 filling scheme the measure of the Beam 2 tune was very noisy (Figure 52). We cannot draw strong conclusions on the tune stability from this specific measurements. Nevertheless the quadrupole feed-forward uses the LHC optics model that has been validated systematically with specific optics measurements.

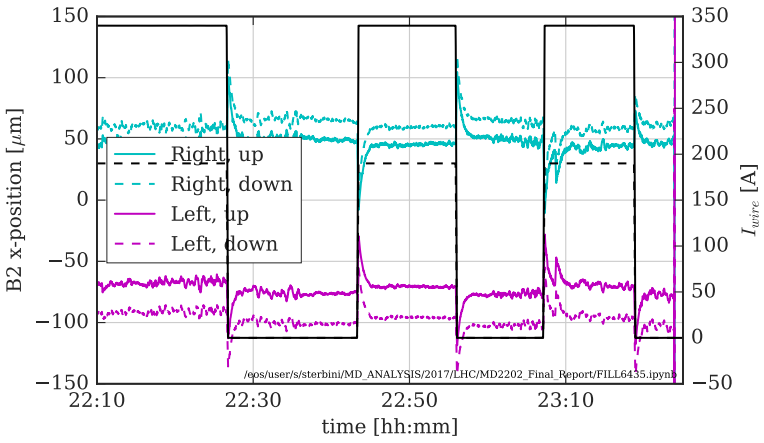

Figure 50: Horizontal closed orbit stability.

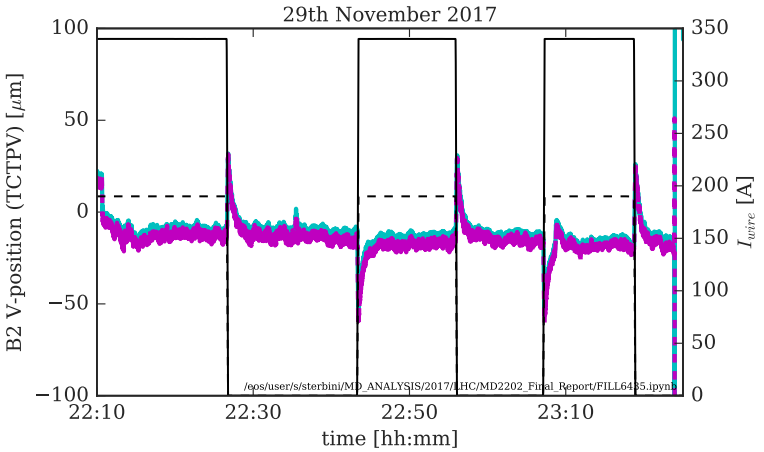

Figure 51: Vertical closed orbit stability.

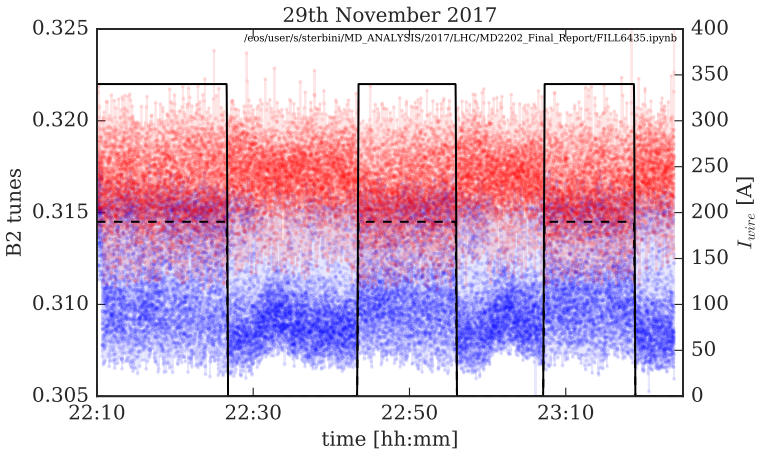

Figure 52: Beam 2 tunes stability.

3.6 The efficiency of the compensation

The results of the MD is reported and commented in this section. By switching on the wires a clear effect was observed in the Beam 2 lifetime, as shown in Figure 53. With the compensation one could increase the Beam 2 lifetime from ≈ 25 h to ≈ 35 h.

It is important to compare the bunch-by-bunch lifetime as shown in Figure 54. The effect on the bunch suffering HO and BBLR (regular bunch) is very clear. The bunch without BBLR (super-PACMAN) is almost not affected at all by the wire compensation. In other words the wire compensation proved to be effective in the MD experimental condition to compensate the regular bunch and, at the same time, did not spoil the performance of the super-PACMAN bunch.

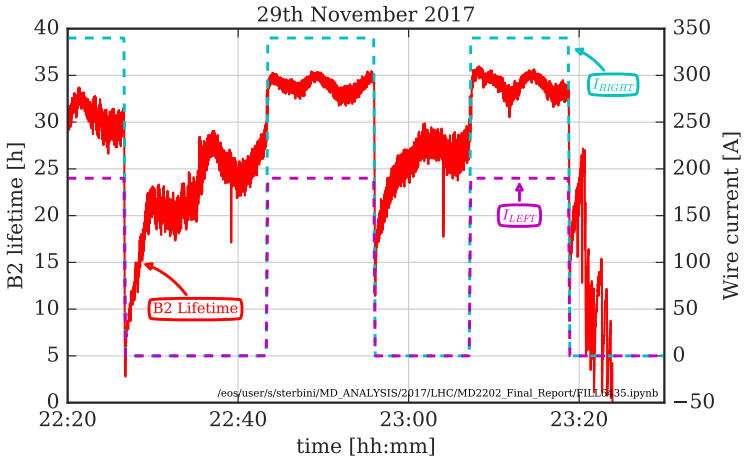

Figure 53: Beam 2 lifetime evolution during the wire compensation.

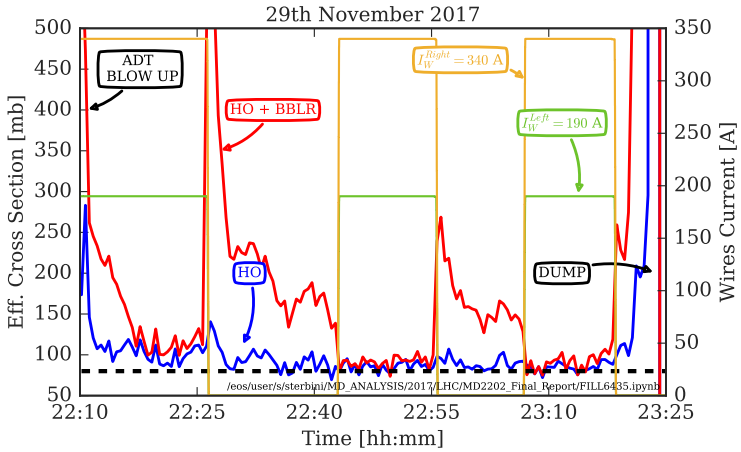

Figure 54: Bunch by bunch lifetime.

4 Conclusions

During the 2017 MD campaign, for the first time it was possible to test DC compensator wires in LHC. These wire prototypes are integrated in the jaws of operational collimators. The prototypes were available only in IR5 (horizontal wires).

The s-position of the wires is close to the ideal one, whilst the transverse distance beam-wire cannot be reduced to the optimal values due to the prototypes constraints. The linear effects of the wire were compensated using dipolar and quadrupolar feed-forwards, in doing so we can directly compare the beam lifetime with and without compensation.

We tested the different optics configurations ($\beta^* = 40$ with $\theta_c/2 = 120$ μrad and $\beta^* = 30$ with $\theta_c/2 = 150$ μrad). **In both cases the wire compensation improved the lifetime of the weak beam (Beam 2). More in details, they improved the lifetime of the regular bunch (the one suffering the HO and LRs) without reducing the lifetime of the super-PACMAN bunch (the one without LRs)**.

We plan to continue the studies in 2018 when two additional wire prototypes will be available in IR1. This will allow to further explore the potential of similar devices for the HL-LHC era.

Acknowledgements

We would like to thank the HL-LHC management together with the HL-LHC Working Group 2, 5 and 13 for their continuous support. We acknowledged the LHC MD coordinators for their active endorsement of the proposed experimental study. We are grateful to all the support received from the Machine Protection Panel and the LHC-OP team.

References

[1] CERN-ATS-Note-2012-072 MD.

[2] W. Herr et al., "Long range beam-beam effects and experience in the LHC", ICFA mini-workshop on "Beam-Beam Effects in Hadron Colliders", CERN, 2013.

[3] T. Pieloni et al., "Two Beam Effects", Proceedings of the Evian Workshop 2014.

[4] T. Pieloni et al., "Beam-Beam Effects Long-Range and Head-on", Proceedings of the Evian Workshop 2015.

[5] M. Crouch et al., "MD 385: Long range beam-beam interaction and the effect on the beam and luminosity lifetimes", CERN-ACC-NOTE-2016-0019.

[6] Y. Papaphilippou, "LHC beam quality and its evolution in 2017", LHC Performance Workshop, Chamonix 2018.

[7] S. Papadopoulou, "Emittance intensity and Lumi modeling and evolution", Proceedings of the Evian Workshop 2017.

[8] J.-P. Koutchouk, "Principle of a Correction of the Long-Range Beam-Beam Effect in LHC using Electromagnetic Lenses", LHC Project Note 223.

[9] S. Fartoukh et al., "Compensation of the long-range beam-beam interactions as a path towards new configurations for the high luminosity LHC", PRST-AB 18, 121001 (2015).

[10] A. Rossi et al., "Installation of two wire collimators in IP5 for Long Range Beam-Beam compensation", EDMS 1705791.

[11] G. Sterbini et al., "MD2202: LR beam-beam compensation", LSWG 17 August 2017, https://indico.cern.ch/event/657430/

[12] https://indico.cern.ch/event/456856/

[13] https://indico.cern.ch/event/615088/

[14] /eos/user/s/sterbini/MD_ANALYSIS/2017/LHC/MD2202_Final_Report

[15] G. Sterbini et al., "Results of the Beam Beam Long Range compensation experiment in LHC", 7th HL-LHC Collaboration Meeting, Madrid, 13-16 November 2017

[16] G. Sterbini et al., "Long-range compensation experiment in the LHC, ICFA Mini-Workshop on Beam-Beam Effect in Circular Colliders", Berkeley, 5-7 February 2018

A Closed orbit feedback analysis

As one can see from Figure 66, during the powering of the wires the Closed Orbit (CO) feedback was on for most of the time. It is important to verify that

- the dipolar feed-forward is working as expected,
- the vertical alignment of the wire is correct (no dipolar vertical kick),
- no H/V dipolar kick is noticeable in Beam 1 when powering the wires.

In order to address the previous points a simple analysis of the beam orbit response is not sufficient since the orbit offset are corrected by the CO feedback. On the other hand one can analyze the time dependence of the kick controlled by the CO system and verify if these kicks are correlated with the wire current. In Figure 55, it is possible to see the correctors kicks variation (with respect to an arbitrary reference time, i.e., 21h35). There is quite an activity of the CO feedback and one can clearly see the corrector 402 and 403 (respectively MCBYH.4L5.B2 and MCBYH.A4R5.B2) reacting against the dipolar kick of the wires. In Figure 56 it is possible to look into the details of three correctors (MCBYH.4L5.B2, MCBYH.A4R5.B2 and MCBYH.4R5.B1). The first two are the one used for the feed-forward. It is possible to observe that the MCBYH.A4R5.B2 is not used by the CO feedback and is following (as expected) the powering cycle of the right wire. The MCBYH.4L5.B2 behavior is dominated by the powering cycle of the left wire. It is possible also to distinguish the luminosity scan trim. It is worth noting (see MCBYH.4L5.B2) that

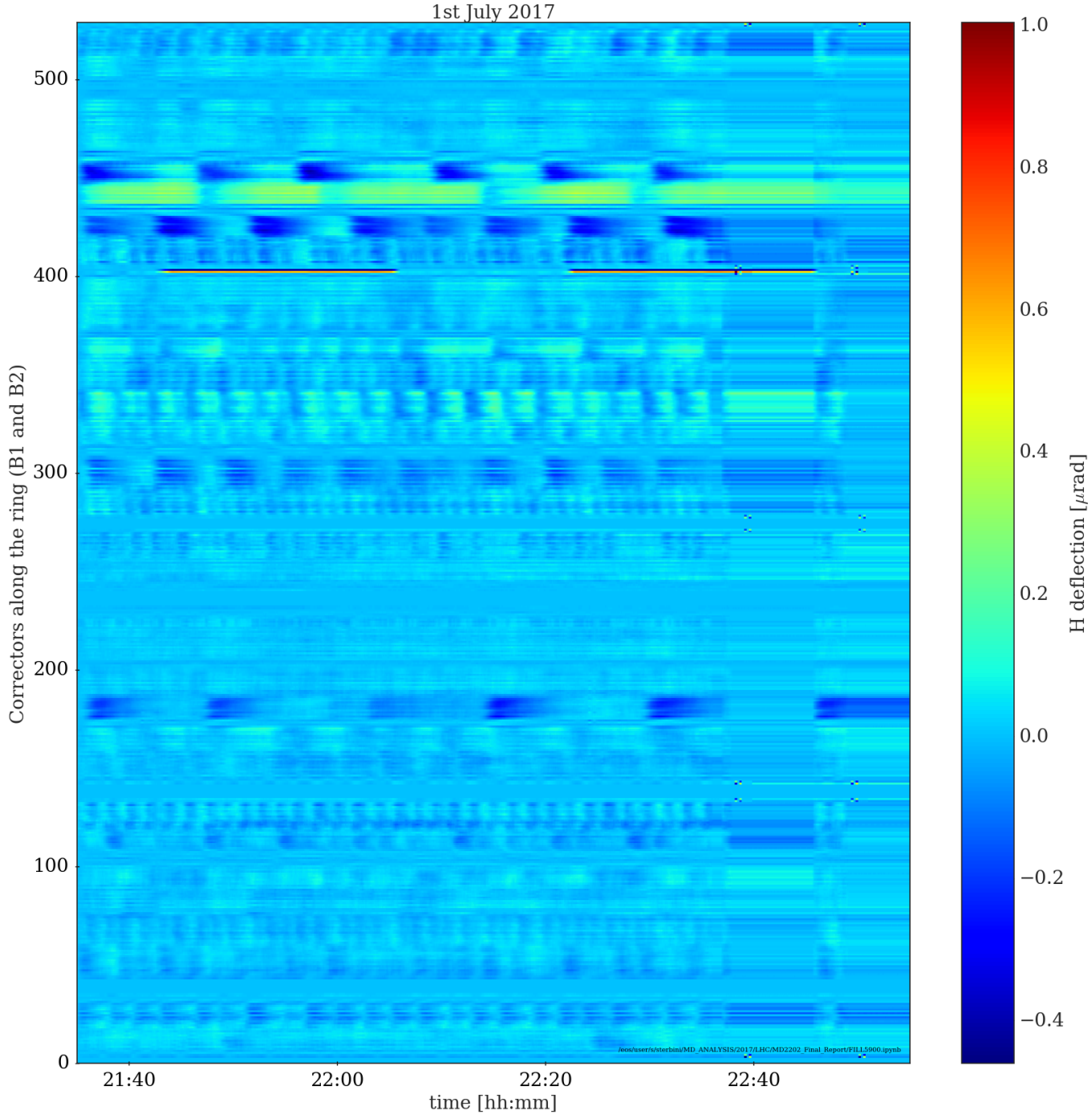

Figure 55: Horizontal correction of the Beam 1 and Beam 2.

the CO orbit correction is oscillating around the feed-forward value and this confirm the correctness of the dipolar feed-forward response. In addition looking, as an example, to MCBYH.4R5.B1 one can conclude that Beam 1 is not experiencing a visible kick.

Similar observation can be done for the vertical plane (Figure 57). In this case, there

is no response of the CO feedback correlated to the wires powering: this confirms the good vertical alignment between the wire and Beam 2.

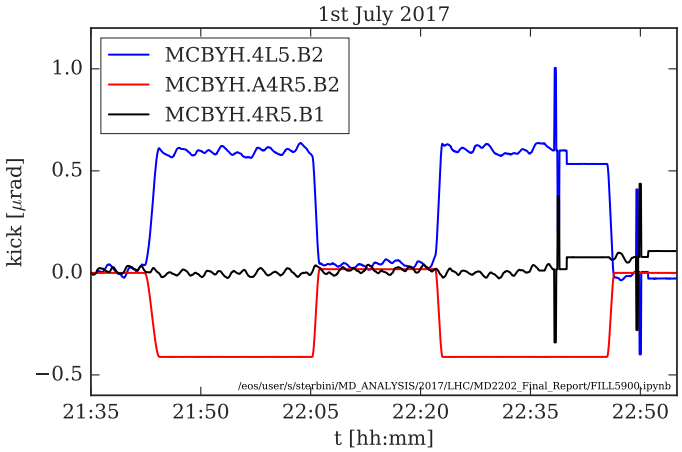

Figure 56: Detail of the horizontal correction of the Beam 1 and Beam 2.

B Complementary plots

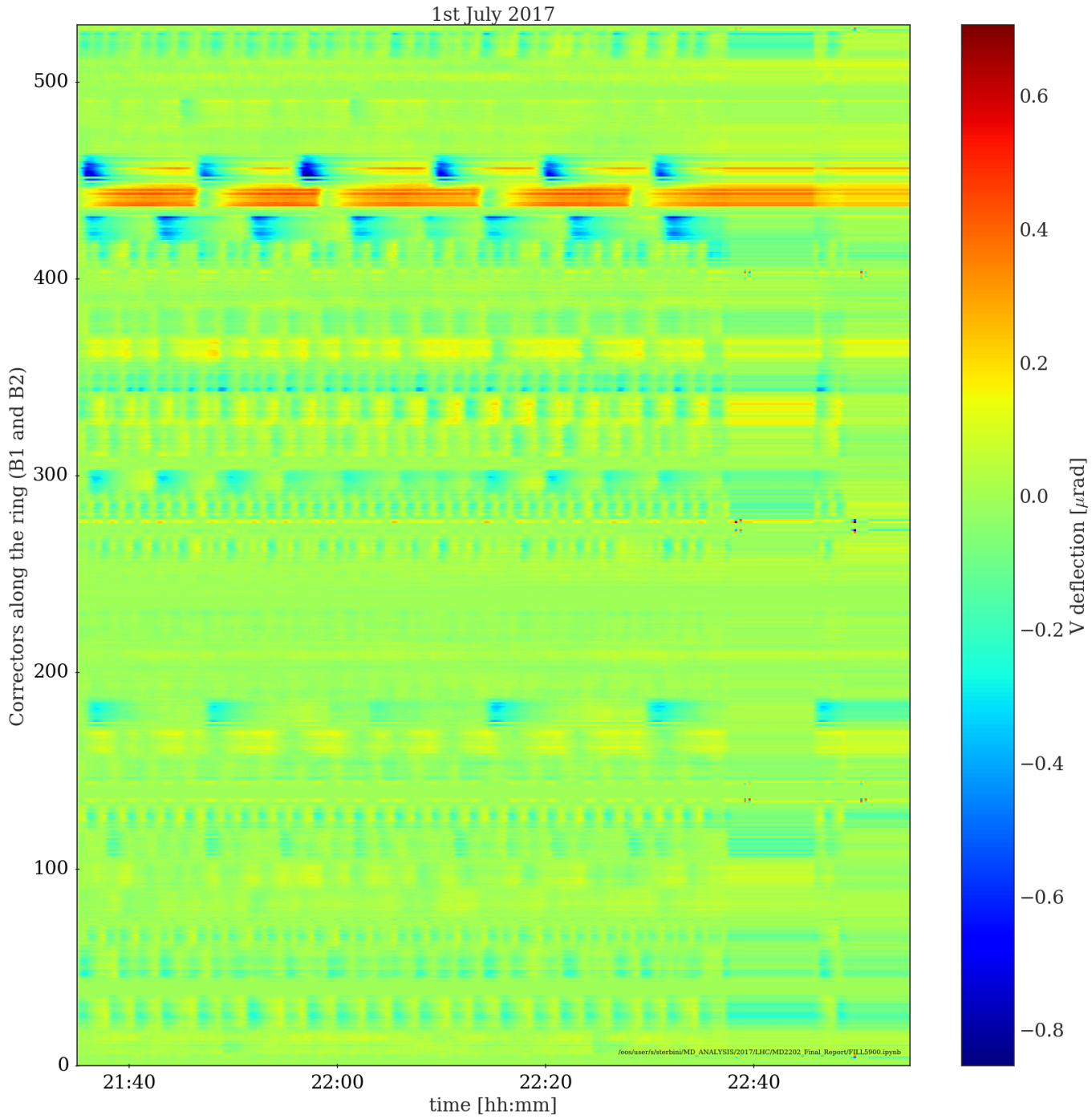

Figure 57: Vertical correction of the Beam 1 and Beam 2.

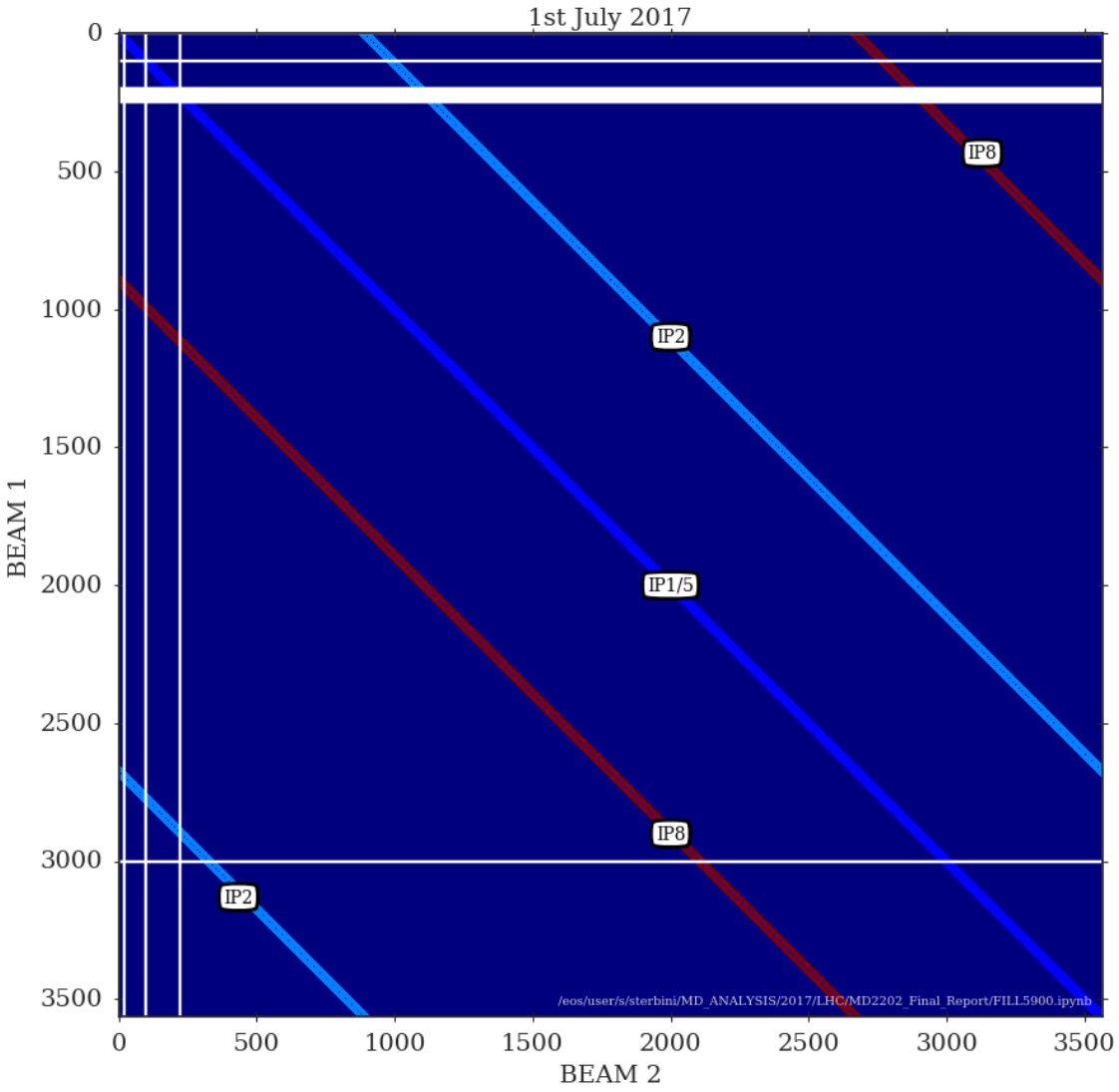

Figure 58: Map of BB encounters.This plot allows by inspection to verify if there are encounters in IR1,2,5,and 8.

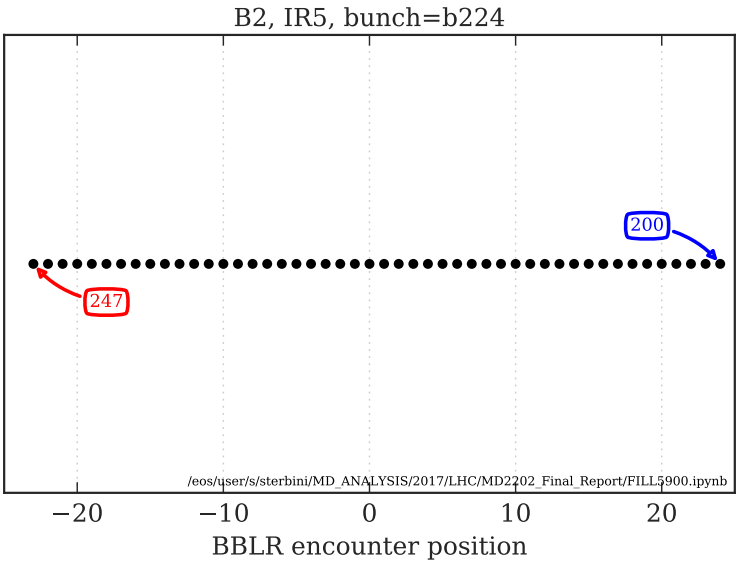

Figure 59: Map of BB encounters.This plot allows by inspection to verify if there are encounters in IR1,2,5,and 8.

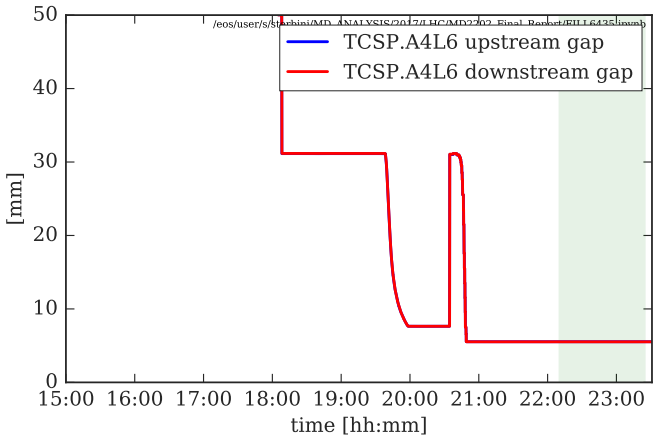

Figure 60: Adjusting the TCSP aperture.

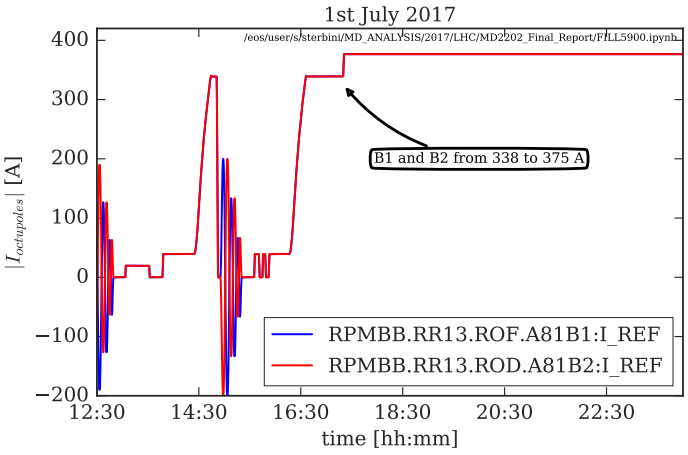

Figure 61: Adjusting the octupoles current.

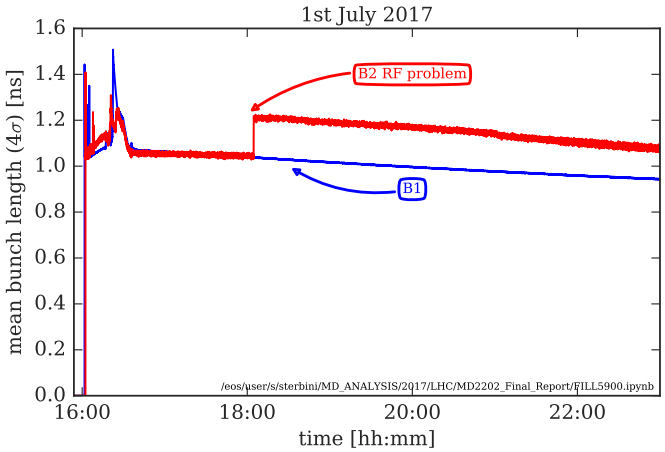

Figure 62: Beam 2 blow up in the longitudinal plane.

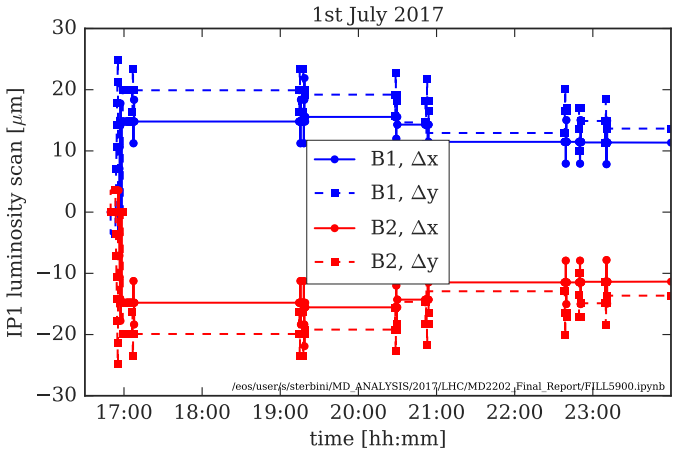

Figure 63: Luminosity scan at IP1.

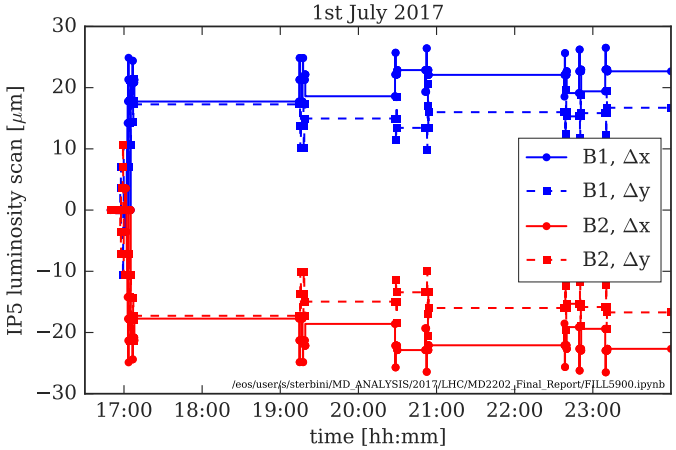

Figure 64: Luminosity scan at IP5.

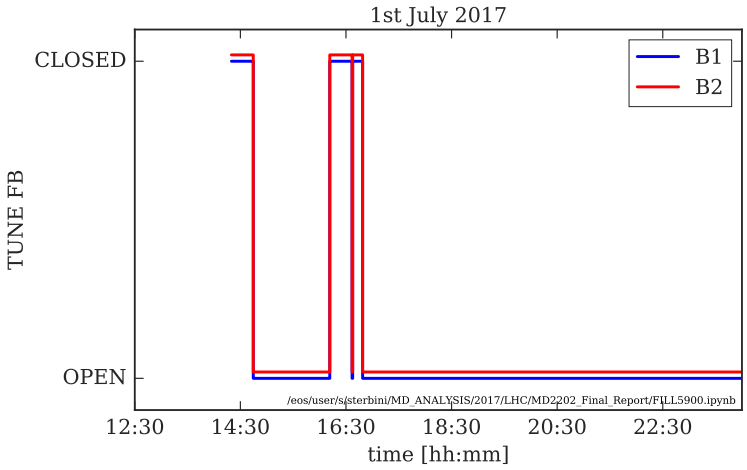

Figure 65: Tune feedback status.

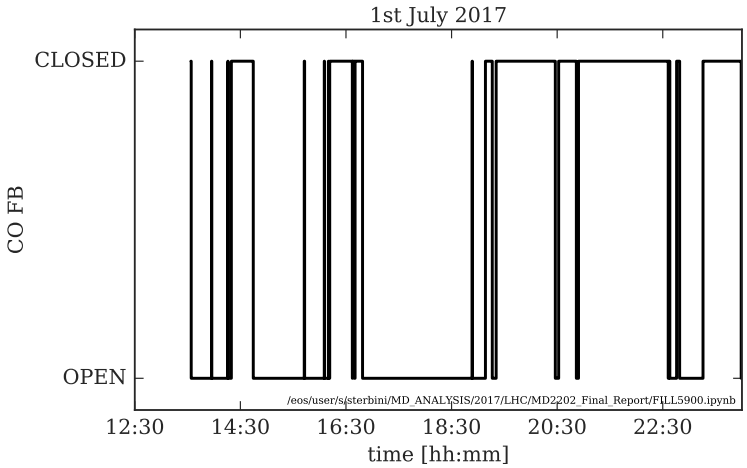

Figure 66: Closed-orbit feedback status.

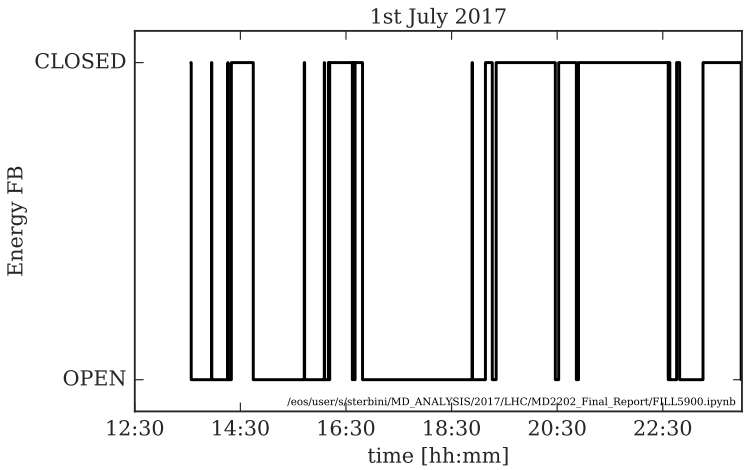

Figure 67: Energy feedback status.

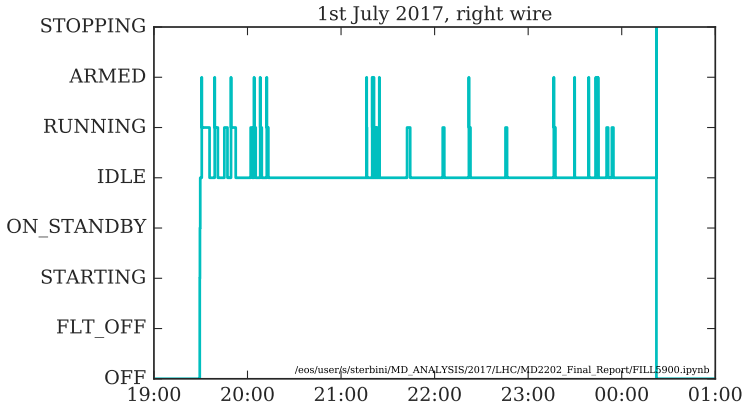

Figure 68: States of the right wire power converter.

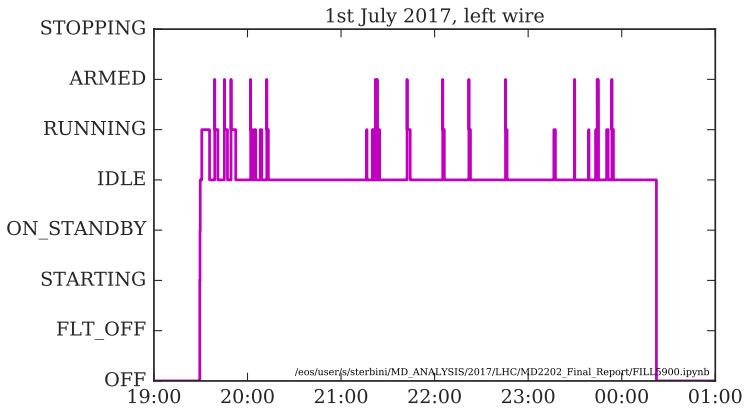

Figure 69: States of the left wire power converter.

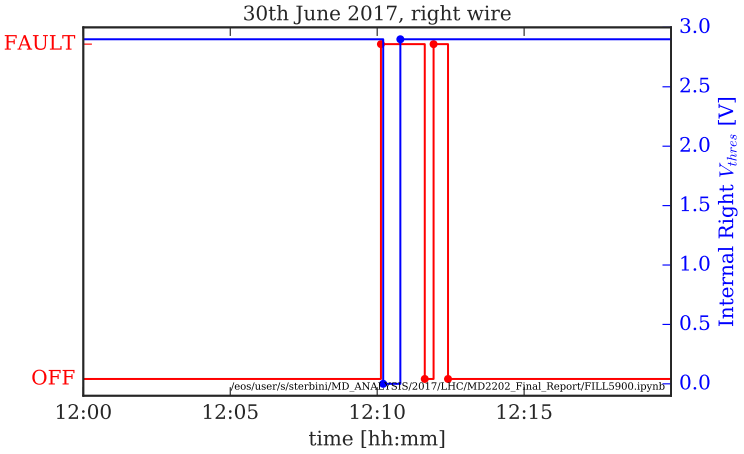

Figure 70: Test of the internal right interlock.

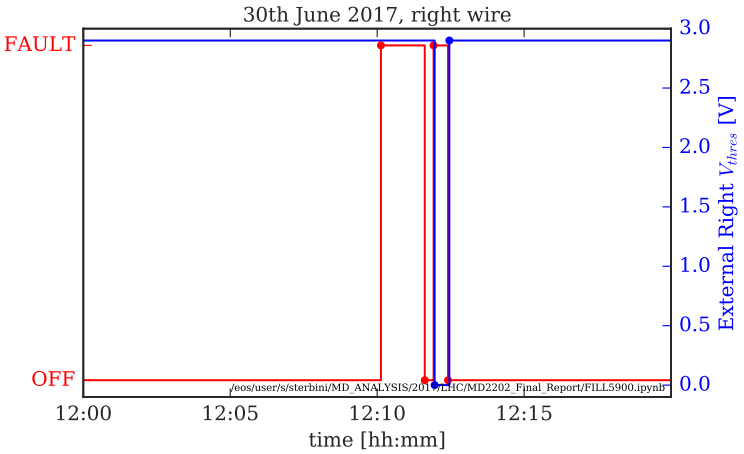

Figure 71: Test of the external right interlock.

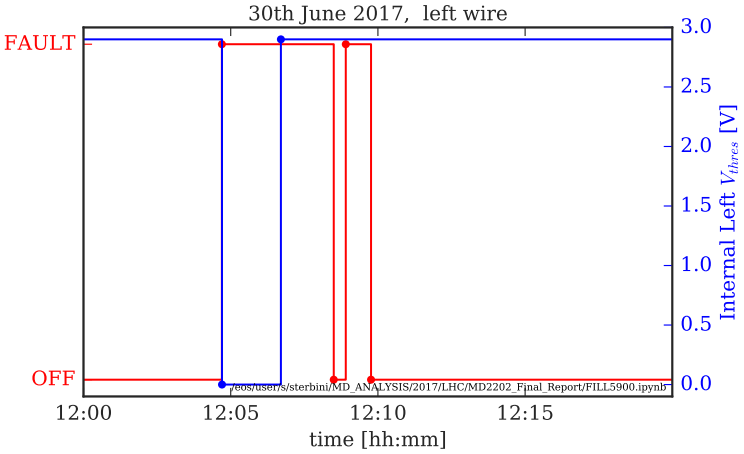

Figure 72: Test of the internal left interlock.

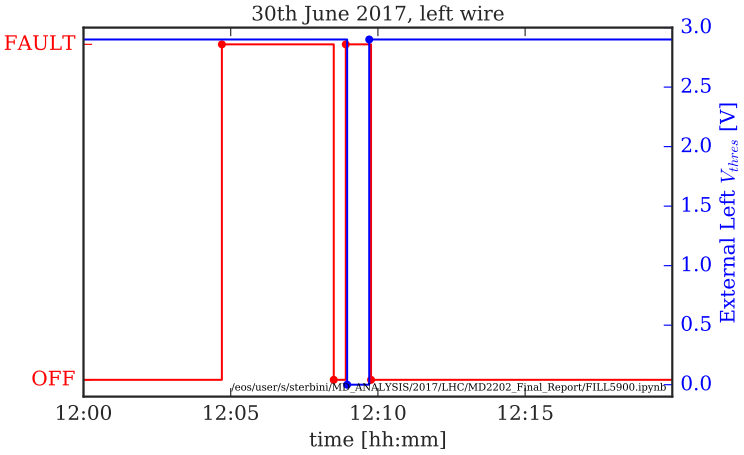

Figure 73: Test of the external left interlock.

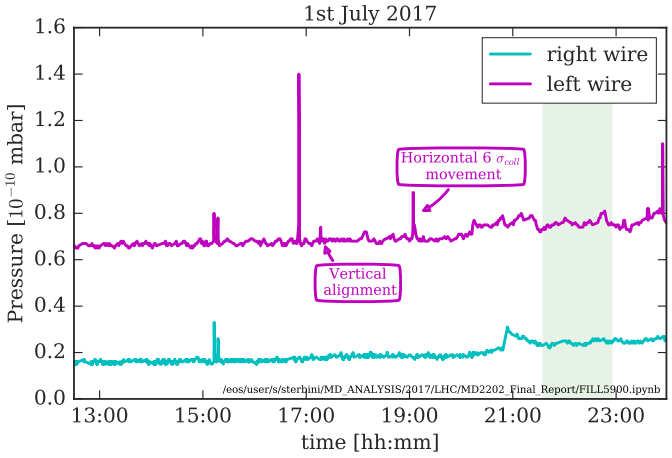

Figure 74: Vacuum level close to the wires during the MD.

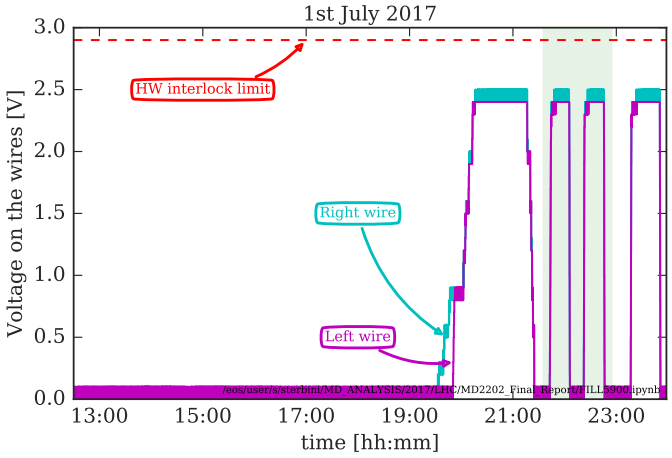

Figure 75: Voltage measured on the internal wires.

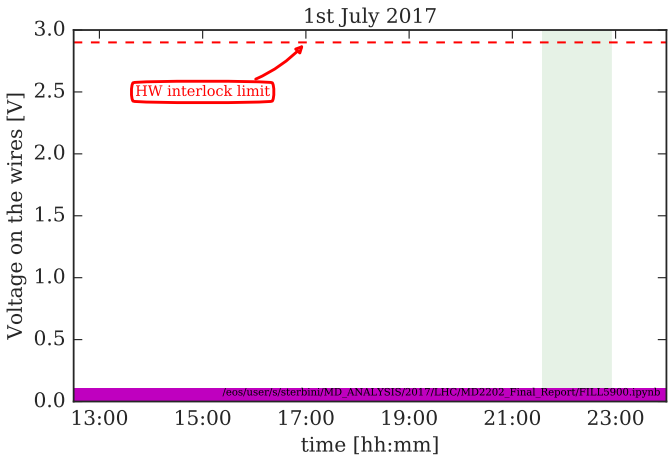

Figure 76: Voltage measured on the external wires (not powered).